

POLITECNICO DI TORINO

Master's Degree in Urban and Territorial Planning

Natural and Anthropogenic Drivers of Groundwater Temperature Variability in Urban Areas: Evidence from the City of Turin

Master's Thesis

Submitted by: Roya Beigpour

Scientific Supervisor: Prof. Giuseppe Mandrone Associate Professor of Applied Geology Interuniversity Department of Regional and Urban Studies and Planning (DIST) University of Turin

Administrative Supervisor: Prof. Stefano Ferrari Interuniversity Department of Regional and Urban Studies and Planning (DIST) Politecnico di Torino / University of Turin Co-supervisor / Scientific

Support: Dr. Jessica Maria Chicco Research Assistant Professor Interuniversity Department of Regional and Urban Studies and Planning (DIST) University of Turin

Academic Year 2026–2027

Dedication

To my brother, Babak,
for always being a source of strength, support, and encouragement throughout my journey.
This thesis is dedicated to you with all my love and gratitude.

abstract

Groundwater temperature is a useful indicator of the interaction between climatic variability, urbanization, and subsurface thermal processes. In urban areas, groundwater thermal conditions may be influenced by natural factors, including groundwater flow, recharge, aquifer properties, and seasonal surface-temperature variations, as well as by anthropogenic factors such as underground infrastructure, impervious surfaces, buildings, and other urban heat sources. This study investigates the spatial and temporal variability of groundwater temperature at five monitoring locations in Turin (Italy), with particular attention to site-specific differences and their surrounding urban context.

The analysis was based on groundwater-temperature records from five piezometers within the Municipality of Turin. Descriptive statistics and monthly mean temperatures were calculated for each monitoring point. Spatial analysis was conducted in QGIS using a consistent 200 m buffer around each piezometer to characterize land use, building height, built-up continuity, and open-space conditions. Four monitoring points were classified as predominantly urban and one as less urban. Because P3 showed a markedly different seasonal pattern from the other sites, an additional analysis was performed using precipitation data from the ARPA Piemonte Torino Via della Consolata station. Contemporaneous and lagged Pearson and Spearman correlations, together with a rainfall-event response analysis, were used to evaluate possible short-term and delayed relationships between precipitation and P3 groundwater-temperature variability.

Mean groundwater temperatures ranged from 13.95 °C at P5 to 17.34 °C at P3, corresponding to a difference of approximately 3.39 °C within the monitoring network. P3 recorded the highest mean temperature and the strongest temporal variability, with lower groundwater temperatures in summer and higher values in winter, whereas P2, P4, and P5 remained comparatively stable. P1 also showed limited variability, although its shorter monitoring period limits direct comparison with the longer records available at the other sites.

The precipitation analysis identified no significant immediate relationship between rainfall and absolute P3 groundwater temperature. However, a weak negative association was observed between precipitation and subsequent daily temperature changes, with the clearest lagged signal occurring approximately 8–10 days after rainfall. The strongest Pearson correlation occurred at a lag of 10 days ($r = -0.201$), while the strongest Spearman correlation occurred at a lag of 8 days ($\rho = -0.270$). Although statistically detectable, these relationships were small in magnitude, and the rainfall-event analysis did not remain statistically significant after correction for multiple testing.

A descriptive comparison showed a mean groundwater temperature of 15.48 °C for P1, P3, P4, and P5, compared with 14.23 °C at P2, corresponding to a difference of approximately 1.25 °C. However, because the less urban category is represented by only one monitoring point and substantial variability

also occurs among the urban sites, this contrast should be interpreted as a local pattern within the monitoring network rather than as evidence of a general urban–less urban thermal relationship or a city-wide subsurface urban heat-island effect.

Overall, the study highlights the value of combining continuous groundwater-temperature monitoring with GIS-based urban characterization and meteorological analysis. The results emphasize the importance of interpreting groundwater-temperature variability at the individual-site scale and of integrating precipitation, groundwater-level, hydrogeological, and subsurface-infrastructure information in future monitoring. Such an approach would provide a stronger basis for distinguishing recharge-related, hydrogeological, and possible anthropogenic influences on groundwater thermal conditions and for supporting future groundwater and shallow-geothermal management in Turin.

Keywords: groundwater temperature; urban groundwater; subsurface thermal variability; Turin; GIS; precipitation; recharge; shallow aquifer; urban hydrogeology; shallow geothermal energy.

Contents

Chapter 1 – Introduction and Conceptual Framework 10
1.1 Background and motivation 10
1.2 Groundwater temperature as an environmental indicator 11
1.3 Drivers of groundwater temperature change 11
1.4 Anthropogenic Drivers of Groundwater Temperature Change 13
1.5 Hydrogeological Controls on Groundwater Temperature 14
1.6 Integrated impacts and conceptual framework 15
1.7 Research objectives and research questions 16
Chapter 2 – Literature Review 17
2.1 Groundwater temperature dynamics and subsurface heat transport 17
2.2 Climate change and long-term groundwater warming 19
2.3 Subsurface Urban Heat Island (SUHI) and anthropogenic heat sources in urban aquifers 21
2.4 Hydrological, ecological, and urban environmental impacts of groundwater warming 22
Chapter 3 – Study Area and Methodology 25
3.1 Study Area: City of Turin 25
3.1.1 Urban Characteristics 27
3.2 Methodological Framework 30
3.3 Assumptions and Limitations 47
Chapter 4 – Results 48
4.1 Spatial and temporal patterns of groundwater temperature in Turin 48
4.1.1 Monitoring periods, data availability, and quality control 48
4.1.2 Descriptive statistics of groundwater temperature 49
4.1.3 Detailed temporal analysis of P3 and meteorological conditions 51
4.1.4 Spatial distribution of mean groundwater temperature 54
4.2 Groundwater temperature characteristics across different urban contexts 55
4.2.1 Classification of the monitoring points by urban context 55
4.2.2 Building-height characteristics around the monitoring points 57
4.2.3 Urban-context classification of the monitoring points 58
4.2.4 Groundwater temperature comparison between urban and less urban contexts 59
4.2.5 Temporal comparison among the monitored contexts 60
4.3 Spatial and Environmental Data Sources: 62
4.4 GIS Environment and Spatial Processing: 63
Chapter 5 – Discussion 64

5.1 Interpretation of groundwater temperature variability in an urban context 64
5.2 Implications for urban planning and groundwater management 67
5.3 Limitations and future research activities 70
Chapter 6 – Conclusions 73
Chapter 7 – References 75

List of Figures

Figure 1. Time series of temperature data with long-term means and observed regime shifts 9
Figure 2. Temporal Response of Groundwater Temperature to Changes in Ground Surface Temperature 11
Figure 3.Conceptual illustration of depth-dependent attenuation and penetration of surface temperature signal. 17
Figure 4. Subsurface temperature anomalies simulated for different subsurface thermal diffusivities. 18
Figure 5. Temperature time series in Switzerland showing atmospheric, river, and groundwater responses to the 1987–1988 climate regime shift.. 19
Figure 6. Schematic representation of urban heat sources affecting groundwater temperature 21
Figure 7. Seasonal temperature attenuation and lag in groundwater discharge. 23
Figure 8. Spatial framework of the study area. 24
Figure 9. Conceptual hydrogeological model of the Turin area 25
Figure 10. Long-term annual temperature trends in Turin during 1870–2014. 26
Figure 11. Land use distribution in Turin, showing urban, industrial, agricultural, and natural areas. 27
Figure 12. Spatial distribution of building height classes in Turin. 28
Figure 13. Spatial distribution and location information of the selected piezometers within the municipal boundary of Turin. 30
Figure 14. Location of Piezometer 1 within the municipal boundary of Turin. 31
Figure 15. Land-use classification within the 200 m buffer area surrounding Piezometer 1. 32
Figure 16. Building-height classification within the 200 m buffer area surrounding Piezometer 1.. 33
Figure 17. Location of Piezometer 2 within the municipal boundary of Turin. 34
Figure 18. Land-use classification within the 200 m buffer area surrounding Piezometer 2. 35
Figure 19. Building-height classification within the 200 m buffer area surrounding Piezometer 2. 36
Figure 20. Location of Piezometer 3 within the municipal boundary of Turin. 37
Figure 21. Land-use classification within the 200 m buffer area surrounding Piezometer 3 38
Figure 22. Building-height classification within the 200 m buffer area surrounding Piezometer 3 39
Figure 23. Location of Piezometer 4 within the municipal boundary of Turin. 40
Figure 24. Land-use classification within the 200 m buffer area surrounding Piezometer 4. 41
Figure 25. Building-height classification within the 200 m buffer area surrounding Piezometer 4.. 42
Figure 26.. Location of Piezometer 5 within the municipal boundary of Turin. 43
Figure 27. Land-use classification within the 200 m buffer area surrounding Piezometer 5. 44
Figure 28. Building-height classification within the 200 m buffer area surrounding Piezometer 5. 45
Figure 29.Monthly mean groundwater temperature trends at the five piezometers 51
Figure 30. Lagged Pearson and Spearman correlations between daily precipitation and subsequent daily changes in P3 groundwater temperature..... 53
Figure 31. Mean change in P3 groundwater temperature following 25 rainfall events with total precipitation ⩾5 mm..... 54
Figure 32. Spatial distribution of mean groundwater temperature at the five monitored piezometers in Turin.... 55

Figure 33.Comparison of mean groundwater temperature between urban and less urban monitoring contexts... 59
Figure 34. Monthly groundwater temperature comparison between urban and less urban monitoring contexts during the common monitoring period 61
Figure 35.Conceptual relationship between urban development, anthropogenic heat sources, groundwater thermal conditions, and geothermal management.. 70

List of tables

Table 1. Percentage distribution of the main land-use categories. 28
Table 2. Distribution of building-height classes. 30
Table 3. Identification codes and locations of the selected piezometers. 31
Table 4. Monitoring period and number of groundwater temperature measurements 49
Table 5. Descriptive statistics of groundwater temperature at the five piezometers. 50
Table 6. Monthly mean groundwater temperature at the five piezometers 50
Table 7. Selected lagged correlations between precipitation and P3 temperature change. 53
Table 8. urban-context classification of the five monitoring points 56
Table 9.Building-height characteristics within the 200 m buffer area around the five monitoring points 57
Table 10. Final urban-context classification of the five monitoring points 58
Table 11. Comparison of mean groundwater temperature between urban and less urban monitoring contexts....59
Table 12. Monthly comparison of groundwater temperature between urban and less urban monitoring contexts during the common monitoring period...……...…….60
Table 13. Spatial and environmental datasets used and processed in this study, including original data sources, data types, and GIS processing steps……..….....62

Chapter 1 – Introduction and Conceptual Framework

1.1 Background and motivation

Over the past few decades, climate change and urban growth have affected how heat moves at the surface. Warmer air from climate change raises ground temperatures, while city pavements and buildings absorb and store more heat. This heat gradually moves into the ground, slowly warming shallow aquifers. Since groundwater temperatures change slowly, they can show long-term environmental trends. Cities play a key role in this process. Urban surfaces stay warmer than green or undeveloped areas, which leads to more heat moving into the ground. Studies have found that Groundwater temperatures in urban areas are often higher than those in nearby rural or less urbanized areas due to anthropogenic heat inputs and modified surface conditions (Ferguson and Woodbury, 2007; Menberg et al., 2013; Zhu et al., 2015). This study aims to fill this gap by using groundwater temperature as an environmental indicator of the combined effects of climate change and increasing urbanization. In particular, urban processes such as greater land use, summer and winter air-conditioning demand, industrial activities, and vehicular traffic may contribute to subsurface thermal alteration and affect shallow aquifers (Taylor and Stefan, 2009; Ferguson and Woodbury, 2007; Menberg et al., 2013).
Figure 1 illustrates examples of groundwater and atmospheric temperature time series, showing how groundwater temperature can record long-term thermal changes and regime shifts.

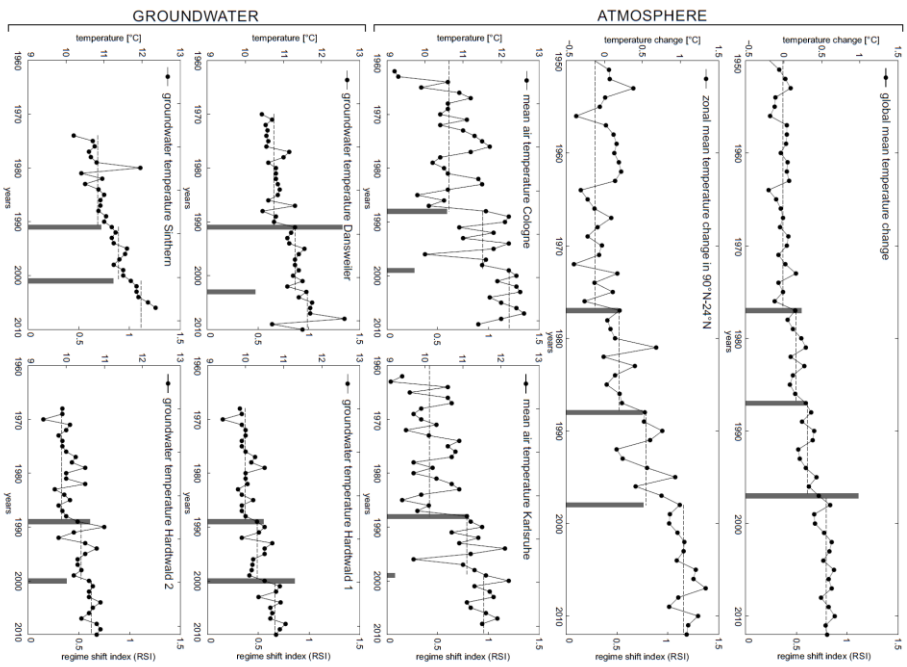


Figure 1. Time series of groundwater and atmospheric temperature data with long-term means and observed regime shifts. Adapted from Menberg et al. (2014).

1.2 Groundwater temperature as an environmental indicator

Groundwater temperature is increasingly recognized as a reliable environmental indicator for tracking long-term changes in both natural and urban environments. Unlike air and surface-water temperature, which can respond rapidly to seasonal and short-term atmospheric variations, groundwater temperature changes more slowly because of the thermal buffering capacity of soils and geological materials. This makes groundwater particularly useful for detecting cumulative thermal signals rather than short-term fluctuations (Taylor and Stefan, 2009; Menberg et al., 2014).

Previous studies have shown that shallow urban aquifers are experiencing increasing groundwater temperatures, with many cases reporting subsurface warming of approximately 2 to 5 K. This subsurface warming is comparable to the atmospheric urban heat island effect, as cities modify the surface energy balance through urban materials and land-cover changes, such as pavements, roads, dense buildings, and sealed surfaces (Zhu et al., 2015; Menberg et al., 2013). Additional anthropogenic heat inputs from buildings, underground structures, basements, district-heating systems, sewer networks, and buried utility systems can further contribute to groundwater warming (Menberg et al., 2013; Benz et al., 2016). These thermal inputs can propagate downward and appear as deviations from natural temperature patterns in borehole and groundwater-temperature records. However, the interpretation of urban groundwater temperature profiles requires caution because heat is transferred through several processes, not only by conduction. Conductive heat transfer transmits surface-temperature signals vertically through the ground, while groundwater flow can redistribute heat through advection. Diffusive and dispersive processes may also smooth or spread thermal signals within the aquifer. As a result, groundwater temperature patterns can vary with depth and location, reflecting the combined influence of surface warming, anthropogenic heat sources, groundwater flow, and local hydrogeological conditions (Anderson, 2005; Bense and Beltrami, 2007).

1.3 Drivers of groundwater temperature change

Climate change exerts a substantial influence on groundwater temperature variability by modifying atmospheric conditions and the hydrological cycle. Sustained increases in air temperature raise ground surface temperatures, which in turn transmit thermal signals into the subsurface via conductive heat transfer. Due to the thermal inertia of soils and geological formations, groundwater temperature responds more slowly and with lower amplitude than atmospheric temperature. Borehole temperature records indicate that persistent surface warming is reflected in subsurface temperature profiles as delayed and attenuated signals, which represent cumulative climatic trends rather than short-term fluctuations. This damping effect becomes more pronounced with depth, making shallow aquifers more sensitive to climate-related thermal forcing, while deeper systems display greater buffering capacity (Huang et al., 2000; Egidio et al., 2022).

In addition to air temperature trends, climate change can indirectly influence groundwater temperature through changes in precipitation, recharge, and snow-related processes. Variations in precipitation amount, intensity, and seasonality affect infiltration dynamics and the transfer of surface thermal signals into shallow aquifers. In cold and temperate regions, rising temperatures can also modify the phase and timing of precipitation by reducing snow accumulation and advancing snowmelt. These changes may increase winter infiltration, while recharge during warmer periods can decrease because of higher evapotranspiration. As a result, groundwater thermal responses are spatially variable and depend on local soil properties, land-surface characteristics, and hydrogeological conditions (Jyrkama and Sykes, 2007).

Cryospheric processes are also important in areas with seasonal snow cover. Snow acts as an insulating layer that limits heat exchange between the atmosphere and the ground during winter. A reduction in snow thickness or duration can weaken this insulation, alter freeze–thaw dynamics, and modify infiltration pathways. These processes influence how thermal signals are transmitted into the subsurface and can affect both the timing and magnitude of groundwater temperature responses. Observational and modelling studies therefore show that changes in snow regimes may contribute to climate-driven groundwater warming and should be considered when interpreting groundwater temperature trends (Kurylyk et al., 2014; Menberg et al., 2014).

Figure 2 shows an example of how groundwater temperature can respond to changes in ground surface temperature over time. The comparison between measured groundwater temperature, assigned ground surface temperature, and predicted groundwater temperature illustrates that groundwater thermal signals are generally delayed and attenuated relative to surface temperature changes. This supports the interpretation of groundwater temperature as a useful indicator of long-term subsurface thermal response.

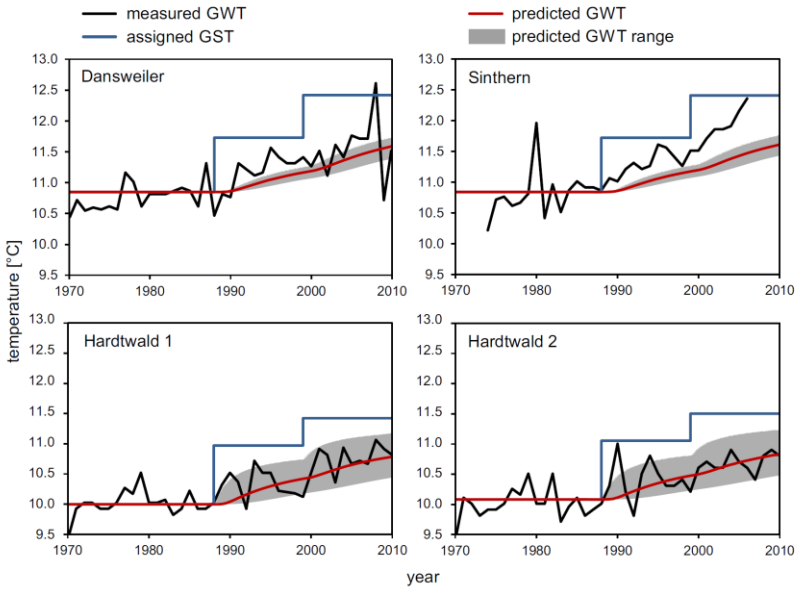


Figure 2. Temporal Response of Groundwater Temperature to Changes in Ground Surface Temperature (Kurylyk et al., 2014; Menberg et al., 2014)

1.4 Anthropogenic Drivers of Groundwater Temperature Change

Groundwater temperature in urban environments is significantly affected by anthropogenic drivers associated with urban development. Urbanization alters land surface properties, energy balances, and subsurface boundary conditions, increasing surface heat storage and promoting downward heat transfer. In contrast to natural geothermal processes, anthropogenic groundwater warming is mainly caused by land surface sealing, built infrastructure, and human-induced modifications of groundwater flow systems. These factors contribute to persistent subsurface warming in densely urbanized areas (Taniguchi and Uemura, 2005). The Subsurface Urban Heat Island (SUHI) effect exemplifies this process, as subsurface temperatures beneath urban cores are consistently higher than those in adjacent rural areas. Ferguson and Woodbury (2007) investigated the subsurface urban heat island in Winnipeg and reported temperature differences of approximately 1–2 K at depths of about 20 m, particularly during winter. Their results showed that these subsurface temperature patterns could not be explained by atmospheric forcing alone, but were also related to local urban factors such as building density, land-use change, and heat losses from infrastructure. This evidence suggests that groundwater temperature can record cumulative anthropogenic heat inputs in urban environments. Urban land surface sealing intensifies subsurface warming by reducing evapotranspiration and increasing both sensible heat flux and heat storage. The substitution of vegetated surfaces with impervious materials leads to persistent near-surface thermal anomalies, which gradually extend into shallow aquifers. This process results in systematically higher groundwater temperatures in developed urban areas (Oke, 1982).

Additional sources of heat include district heating systems, underground infrastructure, groundwater heat pumps, and industrial heat waste. Heat losses from buried infrastructure and the repeated reinjection of thermally altered groundwater create localized yet persistent thermal anomalies in shallow aquifers. In many instances, these anthropogenic heat fluxes surpass natural geothermal heat fluxes, thereby reinforcing the SUHI effect and modifying the long-term thermal regime of urban groundwater systems (Menberg et al., 2013; Benz et al., 2016).

1.5 Hydrogeological Controls on Groundwater Temperature

Natural hydrogeological conditions influence groundwater temperature by regulating the balance between conductive and advective heat transport within the subsurface. Conductive heat transfer mainly controls the downward propagation of surface-temperature variations, including seasonal fluctuations and long-term ground-surface warming. In contrast, groundwater flow can redistribute heat laterally and vertically through advection, thereby modifying temperature–depth profiles. Numerical and analytical studies indicate that even low horizontal groundwater velocities can produce asymmetric and curved temperature profiles, with warming displaced downstream rather than propagating vertically by conduction alone. As groundwater velocity increases, advective heat transport may become dominant, resulting in elongated thermal anomalies and non-linear temperature gradients that differ from those expected under purely conductive conditions (Bredehoeft and Papadopulos, 1965; Bense and Beltrami, 2007).

Aquifer geometry, thickness, and the depth to the groundwater table further influence subsurface thermal responses. Shallow aquifers with a high-water table respond rapidly and strongly to surface temperature changes, while thicker aquifers and deeper groundwater systems display damped and delayed thermal signals that represent long-term average surface conditions. In permeable and sufficiently thick aquifers, surface-induced thermal anomalies can persist for centuries and migrate over distances ranging from hundreds of meters to several kilometers, demonstrating the extended thermal memory of groundwater systems (Kurylyk and MacQuarrie, 2014).

Geological layering and thermal heterogeneity add complexity by influencing both the hydraulic and thermal properties of the subsurface. Differences in thermal conductivity, porosity, and permeability among lithological units affect heat storage and dissipation, frequently resulting in non-linear temperature–depth profiles with slope changes at lithological boundaries. Consequently, groundwater temperature patterns in layered or heterogeneous aquifers can vary substantially over short distances and should not be interpreted solely as direct records of surface temperature history (Clauser and Huenges, 1995).

1.6 Integrated impacts and conceptual framework

Groundwater warming is increasingly recognized as an important process linking climate change, land use, and the functioning of aquatic and groundwater-dependent ecosystems. Rising air and surface temperatures can be transmitted into shallow aquifers, where heat is stored and redistributed through recharge and discharge pathways. This process can affect water resources, river thermal regimes, and groundwater-dependent ecosystems, particularly where warmed groundwater discharges into surface-water systems (Kurylyk et al., 2014; Burns et al., 2017).

Warming can influence both mean groundwater temperature and seasonal variability. Shallow and unconfined aquifers often respond more rapidly and unevenly to surface warming than deeper or confined systems. These systems, especially nutrient-rich floodplain aquifers, may be more sensitive to warming-induced changes in temperature-dependent chemical and biogeochemical processes. As a result, groundwater warming can influence groundwater quality, dissolved oxygen conditions, redox processes, and the mobility of selected dissolved substances (Neidhardt and Shao, 2023).

Beyond thermal increases, groundwater warming accelerates microbial activity and redox transformations, which subsequently affect dissolved oxygen levels, carbon cycling, and solute mobility. These impacts may intensify during heatwaves and droughts, leading to rapid degradation of groundwater quality and reduced resilience of connected surface waters (Neidhardt & Shao, 2023).

The subsurface thermal regime is determined by surface conditions, anthropogenic heat sources, and subsurface heat-transport processes. Atmospheric warming alters ground surface temperature and transmits thermal signals downward primarily through conduction. Groundwater flow redistributes heat via advection and dispersion, thereby influencing the magnitude, timing, and spatial extent of subsurface warming (Menberg et al., 2014). A clear distinction exists between rural and urban groundwater systems. In rural settings, groundwater temperatures are primarily determined by climatic conditions, with seasonal fluctuations diminishing with depth and exhibiting minimal spatial variation. In contrast, urban groundwater is significantly influenced by persistent anthropogenic heat sources, including buildings, paved surfaces, underground infrastructure, and energy systems. These factors elevate baseline groundwater temperatures, generate subsurface urban heat islands, and produce temperature anomalies not attributable solely to atmospheric conditions. Urban groundwater warming is characterized by greater persistence, increased depth of thermal influence, and enhanced heat storage relative to rural areas. As a result, seasonal temperature variations are less pronounced, mean groundwater temperatures are elevated, and thermal recovery periods are prolonged, particularly in shallow and unconfined aquifers. These patterns suggest that urban environments should be conceptualized as systems where human infrastructure and natural processes interact to determine subsurface temperature regimes. This context forms the basis for examining the variability of urban groundwater temperatures in the present study (Taniguchi et al., 2002).

1.7 Research objectives and research questions

The main objective of this thesis is to investigate the spatial and temporal variability of groundwater temperature in the urban area of Turin and to explore how these variations may be related to local urban and hydrogeological conditions. The study focuses on five selected piezometers within the municipal area and combines groundwater-temperature monitoring with GIS-based analysis of the surrounding urban environment. In particular, land use and building-height characteristics are used to describe the urban context around each monitoring point and to support the interpretation of groundwater-temperature differences across the study area.

More specifically, this research aims to:

1. Characterize groundwater-temperature variability at the selected piezometers using descriptive statistics and monthly mean temperatures.
2. Identify spatial differences in groundwater temperature across the monitoring network and compare the thermal behavior of the five monitoring points.
3. Classify the monitoring points according to their surrounding urban context using land-use and building-height characteristics within a 200 m buffer area.
4. Compare groundwater-temperature conditions between predominantly urban and less urban monitoring contexts.
5. Discuss the implications of groundwater-temperature monitoring for urban planning, groundwater management, and the sustainable use of shallow geothermal resources in Turin.

To meet these objectives, the study is guided by the following research questions:

- How does groundwater temperature vary spatially and temporally among the selected monitoring points in Turin?
- What differences in groundwater temperature can be observed among monitoring points characterized by different urban contexts?
- How do the surrounding land-use, building-height, built-up continuity, and open-space characteristics differ among the five monitoring locations?
- To what extent do groundwater temperature patterns differ between predominantly urban monitoring points and the less urban monitoring point during the common monitoring period?
- What implications do the observed groundwater temperature patterns have for urban groundwater management and subsurface planning in Turin?

Chapter 2 – Literature Review

2.1 Groundwater temperature dynamics and subsurface heat transport

Heat transport in groundwater systems is commonly described by the advection–conduction equation, which represents the combined effect of conductive heat transfer through the porous medium and advective heat transport caused by groundwater flow. In a saturated porous medium, the heat-transport equation can be written as:

$$(\rho c)_m \frac{\partial T}{\partial t} = \nabla \cdot (\lambda_m \nabla T) - \rho_w . c_w \, q \cdot \nabla T + Q$$

where T is the groundwater temperature (°C), t is time (s), (ρc) m is the volumetric heat capacity of the saturated porous medium (J m^{-3} K^{-1}), λ_m is the effective thermal conductivity of the saturated porous medium (W m^{-1} K^{-1}), ρ_w is the density of water (kg m^{-3}), c_w is the specific heat capacity of water (J kg^{-1} K^{-1}), q is the Darcy groundwater flux (m s^{-1}), and Q represents an internal or external volumetric heat source or sink (W m^{-3}). The operator ∇ denotes the spatial gradient operator (m^{-1}). The first term on the right-hand side represents conductive heat transfer, while the second term represents advective heat transport associated with flowing groundwater. This formulation is conceptually similar to the solute-transport equation, where conduction is analogous to diffusion and advection depends on groundwater velocity or flux (Anderson, 2005; Bredehoeft and Papadopulos, 1965). Thermal properties do not vary as much as hydraulic conductivity, so temperature data create less uncertainty than hydraulic data alone. This makes heat a reliable natural tracer for tracking groundwater movement. When temperature profiles differ from what is expected from conduction alone, it shows advective flow and can reveal recharge, discharge, and exchanges between groundwater and surface water. If groundwater-flow and heat-transport equations are combined, observed temperature profiles can help constrain possible values of groundwater velocity and hydraulic conductivity (Anderson, 2005). Surface temperature variations propagate downward into the subsurface mainly by heat conduction. As these thermal signals diffuse into the ground, their amplitude decreases with depth, and short-period fluctuations (diurnal and seasonal cycles) attenuate more rapidly than long-term climatic trends. Diurnal signals vanish within the first few meters, seasonal variations within ~10–20 m, while multi-decadal to centennial climate trends can penetrate several hundred meters. Consequently, borehole temperature–depth profiles preserve a record of past ground surface temperature (GST) changes in the subsurface. High-resolution borehole measurements (typically extending to depths of 200–600 m) enable the reconstruction of past surface temperature histories through the inversion of the one-dimensional heat conduction equation. Large-scale geothermal studies demonstrate a clear 20th-century warming signal (~0.5°C), with an overall warming of approximately 1°C over the past five centuries. Therefore,

temperature–depth profiles provide an independent and physically based archive of recent climate variability, complementary to instrumental and proxy climate records (Pollack et al, 1998).

Figure 3 illustrates the conceptual attenuation of surface-temperature signals with depth. Seasonal temperature fluctuations are strong near the ground surface, but their amplitude progressively decreases as heat is transferred downward into the subsurface. This conceptual scheme supports the explanation that shallow groundwater is more affected by seasonal surface-temperature variations, while deeper groundwater mainly records longer-term thermal trends.

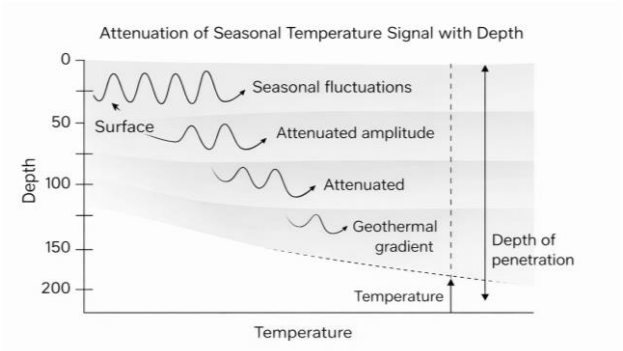


Figure 3. Conceptual illustration of depth-dependent attenuation and penetration of surface temperature signals. Elaborated by the author based on Pollack et al. (1998) and Huang et al. (2000).

The thermal behavior of soils and rocks is governed by three principal properties: thermal conductivity (k), volumetric heat capacity (Cv), and thermal diffusivity (α). These parameters dictate the mechanisms by which heat is transferred, stored, and propagated within the subsurface.

Thermal conductivity is strongly influenced by mineral composition, porosity, and water content. Quartz-rich rocks generally have higher thermal conductivity than feldspar- or clay-rich rocks, reflecting the strong influence of mineral composition on heat transfer. In soils, air-filled pores substantially reduce thermal conductivity, whereas increasing water content and saturation generally enhance conductivity because water conducts heat more effectively than air. Frozen conditions may further increase thermal conductivity because ice has higher thermal conductivity than liquid water (Clauser and Huenges, 1995; Côté and Konrad, 2005), and frozen conditions can further enhance conductivity because ice is a more efficient heat conductor than water. Consequently, thermal conductivity generally increases with greater saturation and reduced porosity.

Volumetric heat capacity ($Cv = \rho c$) quantifies a material' s ability to store heat, where ρ is density and c is specific heat capacity. Saturated soils generally have higher heat capacity than dry soils because water has a high specific heat capacity. Thermal diffusivity ($\alpha = k / Cv$) characterizes the rate at which temperature changes propagate through the ground. Materials with higher diffusivity transmit surface-temperature variations more rapidly and to greater depths (Anderson, 2005; Côté and Konrad, 2005).

2.2 Climate change and long-term groundwater warming

Long-term increases in air temperature modify ground surface temperature (GST), which serves as the upper thermal boundary condition for the subsurface. Under steady-state conditions, where surface temperature and internal geothermal heat flow remain constant, the temperature profile in the upper crust exhibits an approximately linear geothermal gradient. Sustained climatic warming disrupts this equilibrium, generating thermal perturbations at the land surface that propagate downward via conductive heat transfer (Beltrami, 2002). These surface temperature anomalies gradually alter the subsurface temperature field, resulting in deviations from the steady-state gradient that are detectable in borehole temperature profiles. Because heat diffusion in geological media occurs over decadal to millennial timescales, subsurface temperature distributions retain an integrated record of historical changes in the surface energy balance (Huang et al, 2000).

Figure 4 illustrates how surface-temperature changes can appear as subsurface temperature anomalies in borehole profiles. The profile shows that thermal perturbations generated at the land surface do not remain limited to shallow depths, but progressively propagate downward through conductive heat transfer. This supports the interpretation that borehole temperature profiles can preserve long-term signals of past ground-surface temperature change.

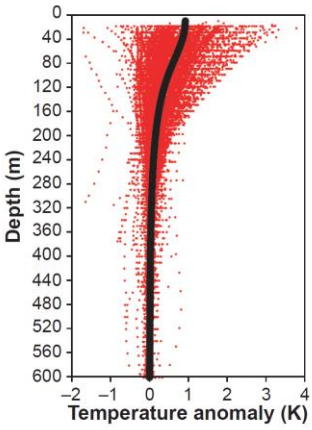


Figure 4. Subsurface temperature anomalies simulated for different subsurface thermal diffusivities. Adapted from Beltrami et al. (2011)

Subsurface and groundwater temperature systems function as long-term archives of past climate conditions rather than merely acting as conductors of heat. Due to the slow movement of heat through geological materials, rapid surface temperature fluctuations dissipate with depth, whereas persistent trends are preserved (Beltrami, 2002). This process attenuates and delays temperature changes, resulting in deeper groundwater temperatures that respond more gradually and with less variability than those near the surface. Consequently, aquifers filter out short-term temperature variations but retain climate signals that persist for decades or centuries. Modeling studies indicate that the depth and duration of these temperature changes are determined by the physical properties of the subsurface and groundwater flow processes (Kurylyk and MacQuarrie, 2014). As a result, groundwater temperature profiles reflect

long-term changes in surface energy and afford valuable information regarding sustained climate warming.

Measured results over recent decades have demonstrated that groundwater systems respond measurably to large-scale climatic forcing. Long-term monitoring of Swiss aquifers recharged by river-bank infiltration identified an abrupt regime shift in groundwater temperature between 1987 and 1988, coinciding with a well-documented Northern Hemisphere climate regime shift linked to changes in the Arctic Oscillation (Figura et al, 2011). Following this variation, annual mean groundwater temperatures increased by approximately 0.7–1.1 K, paralleling increases in regional air and river water temperatures. Cross-correlation analysis showed that groundwater temperatures lagged atmospheric forcing by several months and exhibited reduced variability compared to surface waters. Collectively, these findings deliver immediate empirical evidence that groundwater temperature dynamics are strongly influenced by large-scale climate variability, confirming that aquifers integrate and mirror broader atmospheric regime changes.

Figure 5 presents an example from Swiss aquifers showing how groundwater temperature can respond to large-scale climatic variability. The figure compares atmospheric, river, and groundwater temperature time series and illustrates that groundwater temperature records can reflect climatic regime shifts, although with a delayed and attenuated response compared with surface-water and atmospheric temperature.

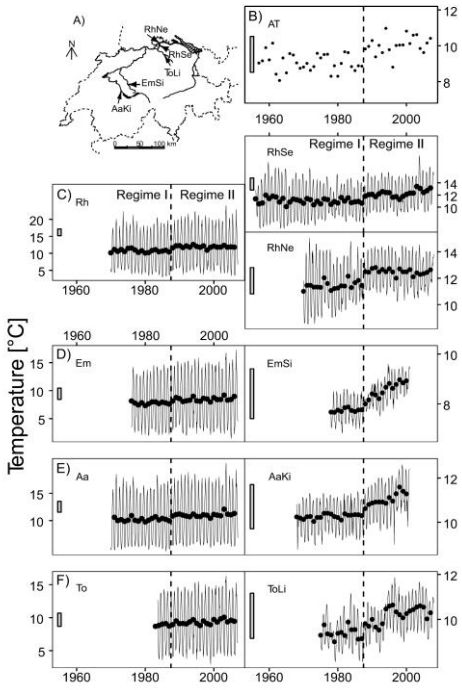


Figure 5. Temperature time series in Switzerland showing atmospheric, river, and groundwater responses to the 1987–1988 climate regime shift. Adapted from Figura et al. (2011).

Recognizing that climate change can warm groundwater is important for understanding hydrogeology. Rising aquifer temperatures are not always caused by local human activity, since large-scale changes in the atmosphere can also affect subsurface temperatures (Figura et al., 2011). Evidence from Swiss

aquifers shows that sudden climate shifts can move through rivers into groundwater, raising temperatures even without urban development. Simulations also show that long-term climate warming alone can change groundwater temperatures and energy storage over large areas (Kurylyk and MacQuarrie, 2014). In fast-growing cities, studies find that subsurface temperatures often reflect both global warming and local heat from urban areas, so it is important to separate these effects (Taniguchi et al., 2007). To accurately interpret groundwater temperature data, researchers need to consider both regional climate changes and local hydrogeological factors to separate global climate effects from urban heat.

2.3 Subsurface Urban Heat Island (SUHI) and anthropogenic heat sources in urban aquifers

Urbanization changes underground temperature patterns, leading to subsurface urban heat islands (SUHIs). Like the better-known urban heat island effect, where cities are warmer than rural areas, SUHI describes how soils and groundwater under cities get warmer because of heat from human activities and changes in how heat moves at the surface (Menberg et al., 2013; Epting and Huggenberger, 2013). In cities, higher ground temperatures and steady heat from buildings and infrastructure cause heat to build up in the shallow ground and aquifers.

Many human activities contribute to SUHI. Heat leaks from buildings, basements, and underground structures, warming the ground. District heating, underground trains, sewage systems, and other buried utilities also release heat into the soil continuously (Menberg et al., 2014). Hard surfaces such as asphalt and concrete make the problem worse by storing heat and reducing cooling from evaporation, which raises ground temperatures and pushes more heat downward.

Literature on subsurface urban heat islands reports that groundwater beneath many cities is becoming warmer. For example, studies in German cities found that groundwater temperatures can be up to 5 °C higher than those in nearby rural areas, highlighting the impact of urbanization on subsurface thermal conditions (Menberg et al., 2013). Similar patterns have been observed in other European cities, where groundwater temperatures tend to be higher in central urban areas and lower toward peripheral zones (Epting and Huggenberger, 2013). These spatial differences can be explained by variations in building density, land-use intensity, impervious surface cover, groundwater depth, and the uneven distribution of anthropogenic heat sources such as basements, district-heating systems, sewer networks, and underground infrastructure.

SUHI affects groundwater systems and how cities manage their environment. Higher groundwater temperatures can change biogeochemical processes, dissolved oxygen levels, and water quality. On the

other hand, the heat stored in urban aquifers could be used as a geothermal energy source for sustainable heating and cooling (Bayer et al., 2019). Understanding how and where SUHI occurs is important for assessing both the environmental effects of urbanization and the potential for using underground heat sustainably.

Figure 6 provides a schematic overview of the main anthropogenic heat sources that can contribute to groundwater warming in urban areas. It shows how dense buildings, basements, underground transport systems, sewer networks, district-heating systems, road tunnels, paved surfaces, and geothermal installations may transfer heat into the subsurface. These sources can increase ground surface temperatures and modify groundwater thermal conditions, especially in dense urban areas where multiple heat inputs are concentrated. The figure therefore supports the discussion of the subsurface urban heat island effect and helps explain how urban infrastructure can influence groundwater temperature.

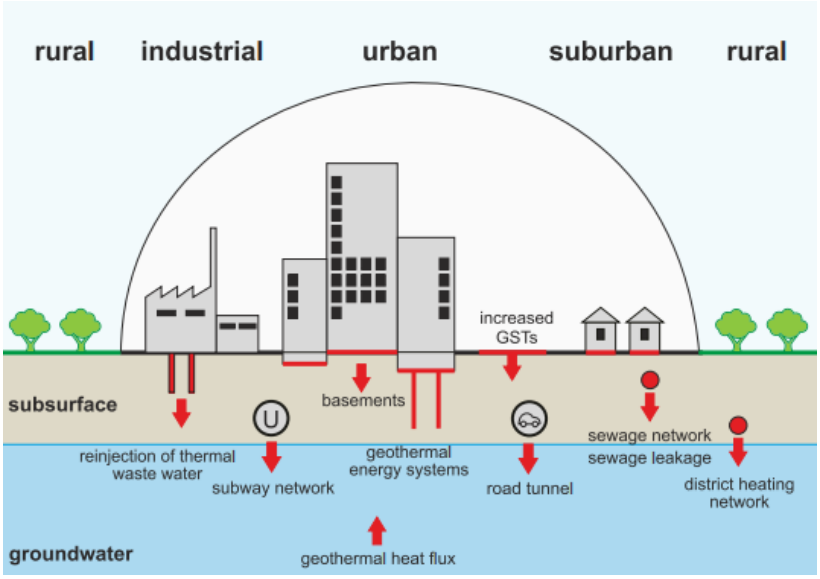


Figure 6. Schematic representation of urban heat sources affecting groundwater temperature. Adapted from Menberg et al. (2013).

2.4 Hydrological, ecological, and urban environmental impacts of groundwater warming

Rising groundwater temperatures significantly influence hydrogeological processes, groundwater quality, and urban environments. Because temperature governs fluid movement and heat transfer, increased groundwater temperatures alter subsurface water flow and the distribution of thermal energy within aquifers. Elevated temperatures accelerate heat transport, modify groundwater flow patterns, and

generate thermal anomalies that propagate through aquifer systems. Empirical studies indicate that persistent surface warming alters subsurface temperature regimes and groundwater heat storage, potentially affecting aquifer recharge and the broader thermal structure of groundwater systems (Kurylyk et al., 2014; Anderson, 2005).

Groundwater temperature is a key determinant of hydro chemical conditions. Numerous geochemical reactions within aquifers are temperature-dependent; thus, rising groundwater temperatures accelerate biogeochemical processes and alter redox conditions. Increased temperatures enhance reaction rates, affect mineral dissolution and precipitation, and influence the mobility of dissolved solutes. For example, higher groundwater temperatures stimulate microbial activity and may result in the release or precipitation of redox-sensitive elements such as iron and manganese, which serve as important indicators of groundwater quality. Empirical data from European aquifers demonstrate that groundwater warming linked to climatic variability can modify biogeochemical conditions and potentially impact the suitability of groundwater for drinking water supply (Figura et al., 2011; Bonte et al., 2013).

In addition to hydro chemical effects, groundwater warming can impact subsurface ecosystems and groundwater-dependent environments. Temperature serves as a fundamental environmental variable that regulates microbial metabolism, biodiversity, and ecological processes within aquifers and hyporheic zones. Variations in groundwater temperature can shift microbial community composition, alter oxygen dynamics, and influence the functioning of groundwater-dependent ecosystems. These effects may extend to surface water systems via groundwater–surface water interactions, thereby affecting ecological conditions in connected rivers and wetlands (Brielmann et al., 2009; Hannah et al., 2009).

In urban settings, groundwater warming presents significant challenges for water resource management and urban infrastructure. Elevated groundwater temperatures can impact drinking water supply systems, influence groundwater monitoring protocols, and affect the performance of shallow geothermal technologies for heating and cooling. Additionally, anthropogenic heat inputs from buildings, subsurface infrastructure, and district heating systems intensify temperature increases in urban aquifers, resulting in the formation of subsurface urban heat islands (SUHI). Therefore, a comprehensive understanding of the combined effects of climate-induced warming and urban heat emissions is crucial for sustainable groundwater management in cities and for assessing both the risks and opportunities associated with the thermal utilization of groundwater resources (Menberg et al,2013; Bayeretal,2019).

Figure 7 illustrates how groundwater temperature can be delayed and attenuated compared with air and ground-surface temperature. The figure shows that seasonal temperature variations at the surface are not transferred immediately to groundwater; instead, the groundwater response depends on aquifer configuration, recharge conditions, groundwater flow, and snowpack insulation. This supports the idea

that groundwater systems can smooth short-term atmospheric fluctuations and record delayed subsurface thermal responses.

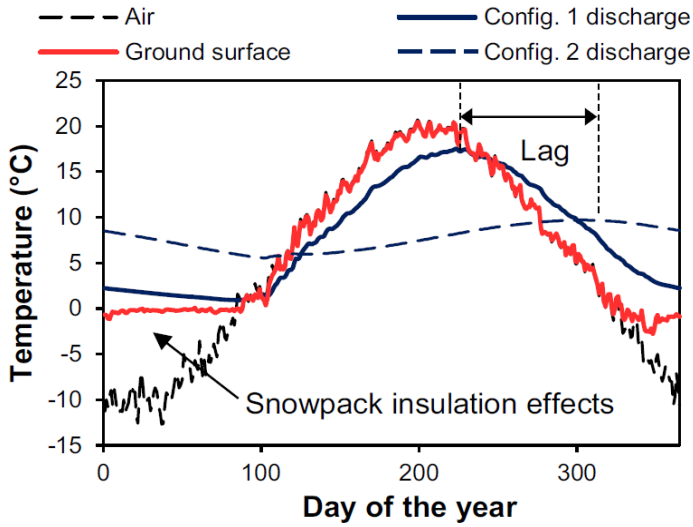


Figure 7. Seasonal temperature attenuation and lag in groundwater discharge. Adapted from Kurylyk et al. (2014)

Chapter 3 – Study Area and Methodology

3.1 Study Area: City of Turin

Turin is situated in the Piedmont region of northwestern Italy and constitutes part of the Turin–Cuneo plain within the western Po Plain. Regionally, the study area spans an elevation range from approximately 600 meters above sea level in the southern sector to around 200 meters above sea level in the eastern sector (Forno et al., 2018). Figure 8 shows the location of Turin in northwestern Italy and the municipal boundary of the study area, providing the geographical context for the groundwater analysis.

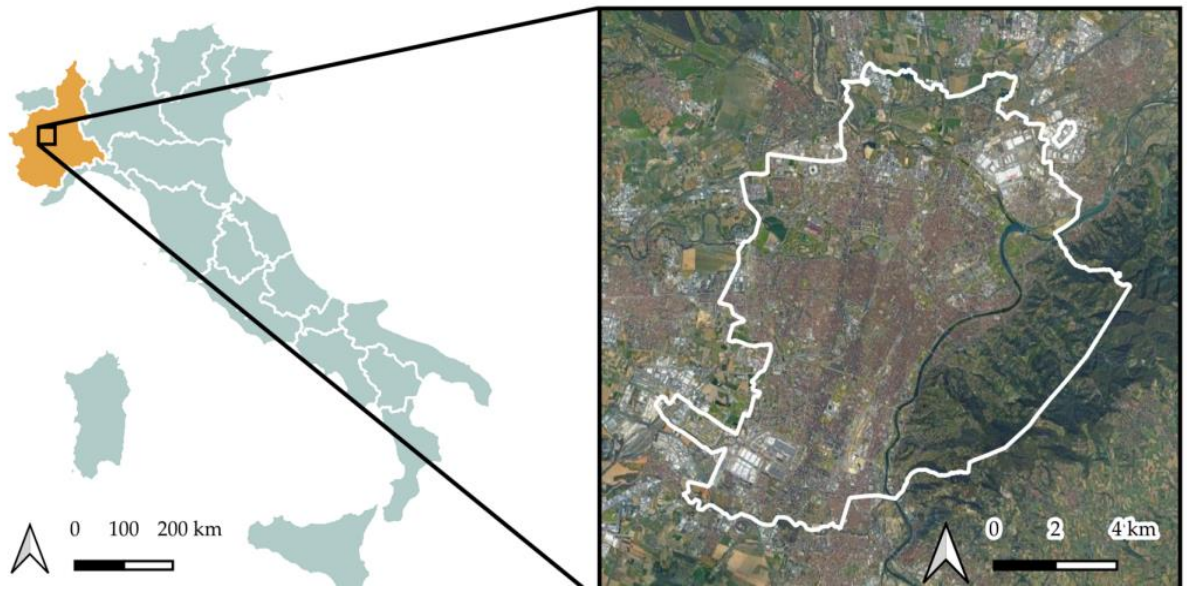


Figure 8. Spatial framework of the study area. (Chicco et al., 2026)

Hydro geologically, Turin is characterized by a multilayer aquifer system developed within Quaternary fluvial and glaciofluvial deposits. Groundwater generally flows from the western Alpine sector towards the east, following the regional topographic gradient and converging towards the Po River. It includes a shallow unconfined aquifer hosted in highly permeable outwash and fluvial deposits and deeper confined or semi-confined aquifers separated by low-permeability layers. Groundwater recharge mainly occurs in the western sector near the Alpine front, while discharge takes place towards the eastern part of the basin and along the Po River corridor (Forno et al., 2018).

Figure 9 presents the conceptual hydrogeological model of the Turin area proposed by Forno et al. (2018). The model shows the main shallow and deep groundwater flow circuits from the western Alpine sector towards the eastern part of the basin and the Po River corridor. It also highlights the role of the glacial, outwash, fluvial, and marine sedimentary complexes in controlling groundwater circulation.

This figure is useful for interpreting the hydrogeological context of the study area, as it illustrates the multilayer aquifer system and the general west–east groundwater flow direction beneath Turin.

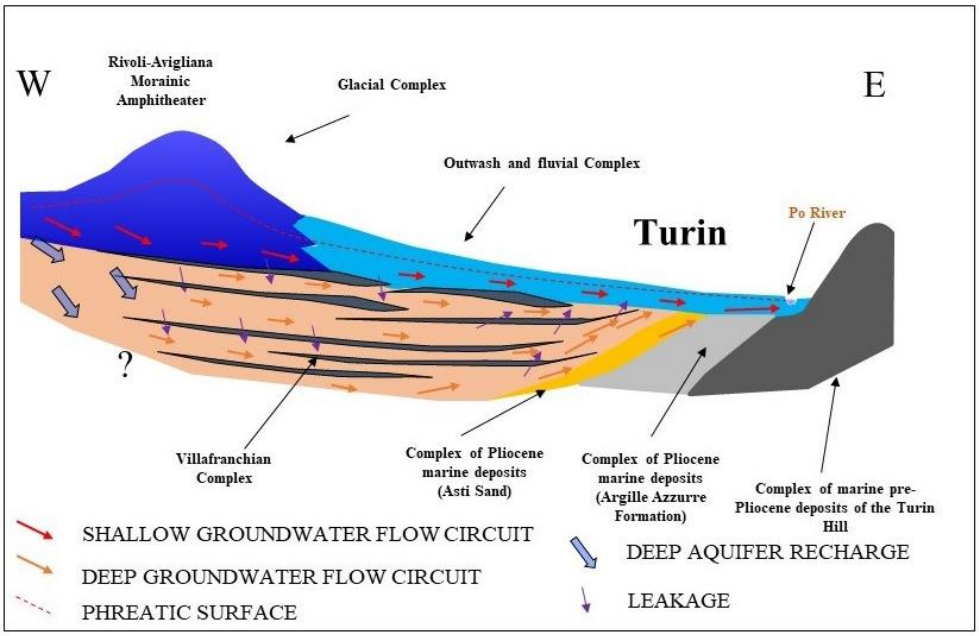


Figure 9. Conceptual hydrogeological model of the Turin area (Forno et al. 2018).

Turin has a temperate climate marked by warm summers and relatively cold winters. Long-term meteorological observations show that the city possesses one of the longest climate data series in Italy, with temperature and precipitation records extending back approximately 260 years. Over the period 1870–2014, mean temperature in Turin increased by about 3.4 °C, with considerable rises in maximum and minimum temperatures. In contrast, rainfall trends do not show significant long-term changes in total wet-day precipitation or rainfall intensity. These long-term warming trends provide an important climatic context to understand groundwater temperature variations within the monitored urban aquifer system (Garzena et al., 2019).

Figure 10 shows the long-term annual temperature trends in Turin between 1870 and 2014, including maximum temperature (TX), minimum temperature (TN), mean temperature (TM), and the linear trend of mean temperature. The figure highlights a clear warming trend over the observation period, especially from the second half of the twentieth century onward. This long-term climatic context provides a general background for the present study and supports the subsequent interpretation of groundwater-temperature variability in relation to meteorological conditions.

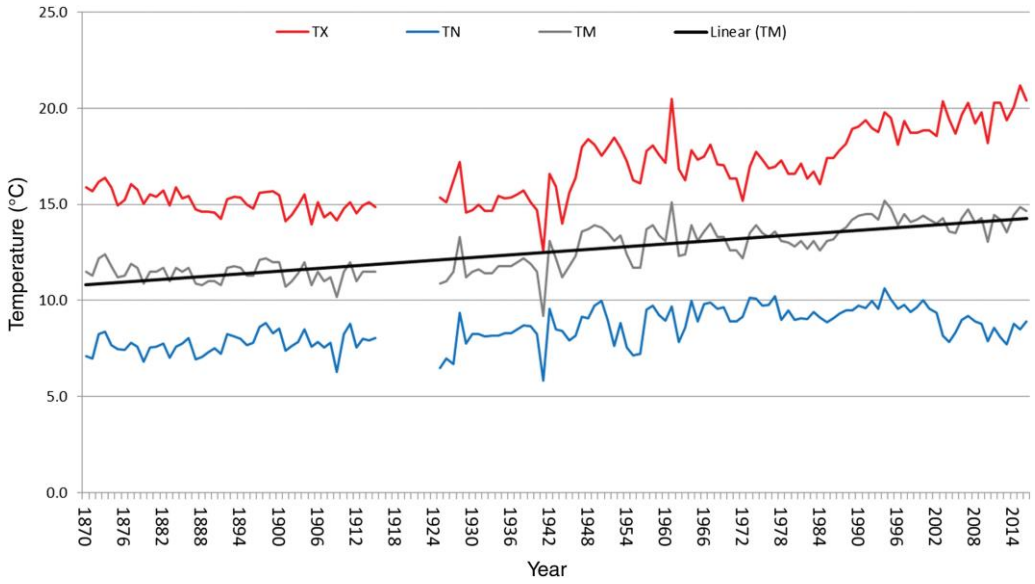


Figure 10. Long-term annual temperature trends in Turin during 1870–2014. Adapted from Garzena et al. (2019).

3.1.1 Urban Characteristics

Land use in Turin is characterized primarily by urban and industrial development, especially in the central and western sectors. Green and natural areas are concentrated along the Po River corridor and in the eastern part of the municipality. Agricultural zones are predominantly situated in the peripheral areas. Figure 11 presents the spatial distribution of the principal land use categories within the study area, offering an overview of the urban landscape surrounding the monitored groundwater system.

Figure 11 shows the spatial distribution of the main land-use categories within the municipal area of Turin. The map highlights the predominance of urban and industrial/commercial surfaces in the central and western parts of the city, while forest and natural areas are mainly concentrated along the eastern hilly sector and near the Po River corridor. Agricultural land and urban green areas appear more discontinuously, mostly in peripheral or transitional zones. This land-use characterization provides a spatial description of the urban environment and supports the comparison of local surface and built-environment characteristics surrounding the monitoring locations.

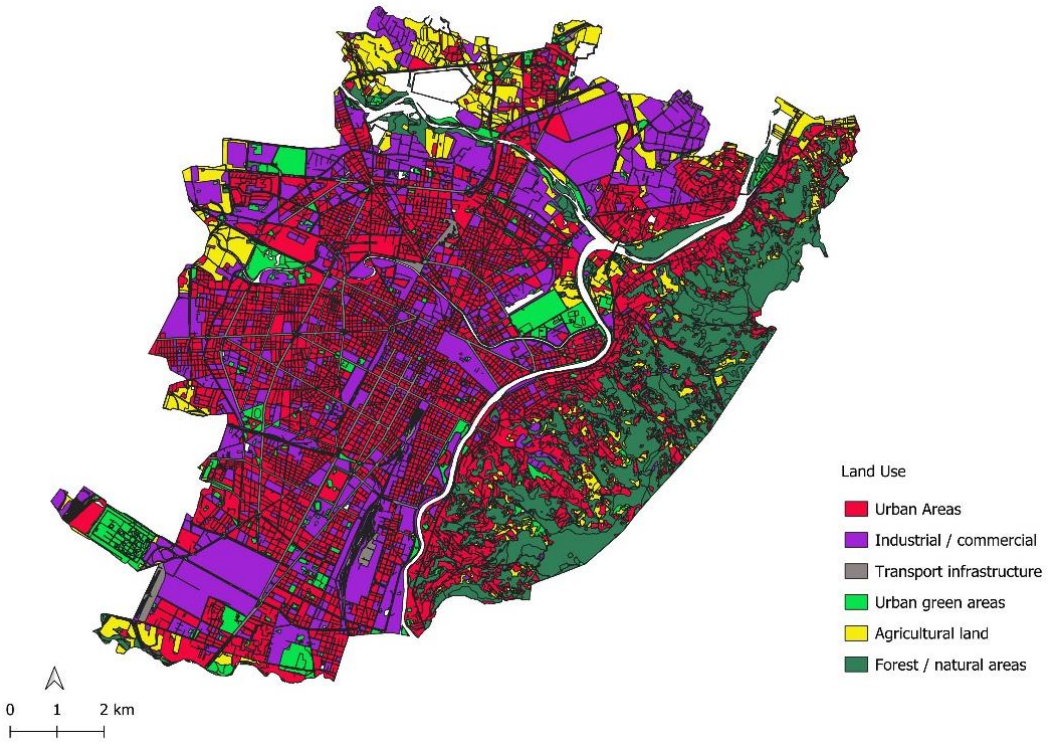


Figure 11. Land use distribution in Turin, showing urban, industrial, agricultural, and natural areas. (Author's elaboration based on Land Cover Piemonte 2023 data from Regione Piemonte Geoportale.)

Table 1 reports the percentage distribution of the main land-use categories within the study area. The results show that artificial surfaces represent the dominant land-use category, accounting for 74.16% of the municipal area. Forest and natural areas cover 15.90%, while agricultural areas and water bodies represent smaller shares, equal to 7.52% and 2.43%, respectively. This confirms the strongly urbanized character of the study area and provides a quantitative basis for interpreting the land-use map shown in Figure 11.

Category	Area share (%)
Artificial surfaces	74.16
Forest and natural areas	15.90
Agricultural areas	7.52
Water bodies	2.43

Table 1. Percentage distribution of the main land-use categories within the study area, calculated by the author using GIS analysis of the land-use dataset described in Chapter 3.

The spatial distribution of building heights in Turin demonstrates a predominance of low- to medium-rise structures throughout the urban fabric. Residential zones primarily consist of buildings ranging from 1 to 7 floors, which suggests a dense yet horizontally extensive urban morphology.

Taller buildings, normally ranging from 8 to 18 floors or more, are concentrated in specific areas, especially within industrial and large-scale commercial districts in the southern and north-eastern sectors of the city. These structures most likely correspond to industrial complexes, warehouses, public facilities, and isolated high-density developments.

The central urban core displays a continuous and homogeneous distribution of medium-height buildings, indicating the historical consolidation and dense urban structure of Turin. Conversely, peripheral areas exhibit a fragmented spatial pattern characterized by lower building density and greater variability in building heights.

Figure 12 shows the spatial distribution of building-height classes within the municipal area of Turin. The map indicates that medium-height buildings, particularly those with 4–7 floors, are widely distributed across the central urban area, reflecting the compact and consolidated built fabric of the city. Taller buildings, including 8–18 floors and 19+ floors, appear more locally concentrated, especially in specific residential, commercial, or large-scale urban development areas. In contrast, peripheral zones show a more fragmented pattern, with lower building density and greater variability in building height. This building-height characterization provides a general description of the urban morphology of Turin and supports the spatial characterization of the built environment surrounding the monitoring locations.

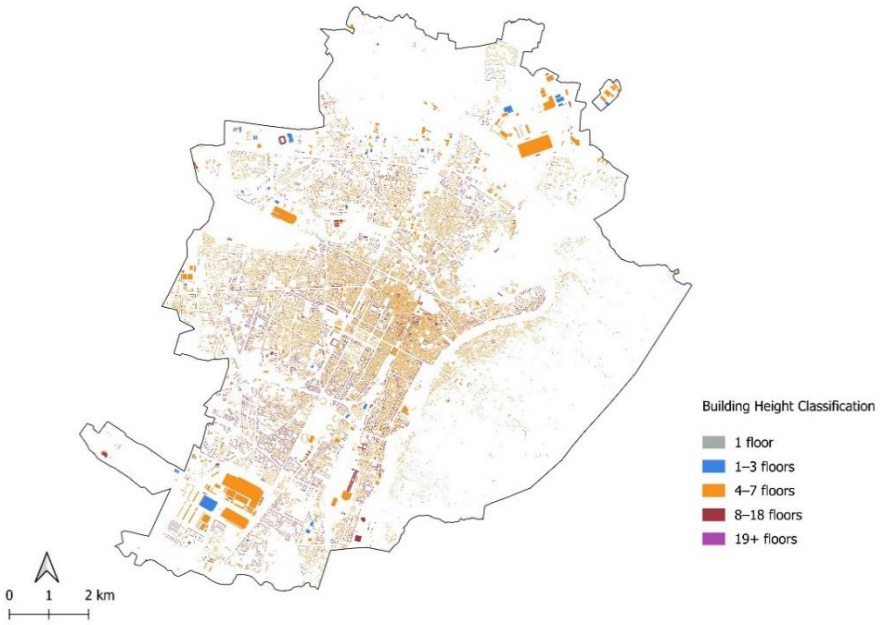


Figure 12. Spatial distribution of building height classes in Turin. (Author's elaboration based on Land Cover Piemonte 2023 data from Regione Piemonte Geoportale.)

Table 2 summarizes the distribution of building-height classes within the study area. The results show that buildings with 4–7 floors represent the dominant class, accounting for 66.5% of the total building stock. Buildings with 2–3 floors represent 22.4%, while taller buildings with 8–18 floors account for 10.3%. Very low-rise buildings with 1 floor and very tall buildings with 19 or more floors represent only minor shares, equal to 0.7% and 0.1%, respectively. These results confirm that Turin is mainly characterized by a medium-rise urban fabric, with taller buildings concentrated only in specific areas.

Building class	count	Percentage (%)
1 floor	257	0.7
2–3 floors	7,903	22.4
4–7 floors	23,475	66.5
8–18 floors	3,625	10.3
19+ floors	25	0.1

Table 2.Distribution of building-height classes within the study area, calculated by the author using GIS analysis of the building-height dataset described in Chapter 3.

3.2 Methodological Framework

The piezometers examined in this study are components of the groundwater monitoring network managed by the Municipality of Turin. A subset of five piezometers was selected based on spatial and technical criteria.

The selected monitoring points are primarily situated in the southern sector of the city, which facilitates consistent spatial comparison within a relatively homogeneous urban context. Simultaneously, the monitoring network retains a distributed spatial configuration across various urban areas, ensuring representative coverage of diverse local environmental conditions. The 200 m buffer was selected to represent the immediate surroundings of each monitoring point while maintaining a sufficiently local spatial scale to distinguish differences in land use, urban morphology, and built-up continuity among the five sites. The buffer was therefore used as a consistent spatial unit for comparative urban analysis and should not be interpreted as a direct hydrogeological or thermal influence radius.

An additional criterion considered in the selection of the monitoring points was piezometer depth. The selected piezometers represent relatively shallow monitoring locations, although their total depths are not identical. The approximate depths are 25 m for P1, 28 m for P2, 26.5 m for P3, 36 m for P4, and 41.5 m for P5. These differences were retained in the study because the available monitoring network

did not provide five sites with identical depths and comparable spatial coverage. Consequently, piezometer depth is considered a site-specific characteristic that may contribute to differences in groundwater thermal response and is taken into account when interpreting the results. Groundwater temperature data for all five monitoring points were collected using Mini-Diver data loggers. The instruments recorded both temperature and pressure; however, only groundwater temperature data were used for the analyses presented in this study. Where available, pressure records were used during data-quality control to help identify periods associated with sensor removal, reinsertion, or stabilization.

Table 3. reports the identification codes and locations of the five selected piezometers used in this study. These monitoring points were selected according to their spatial distribution, data availability, and comparable well depth.

Piezometer ID	Location
P1	Corso Massimo D'Azeglio, 21
P2	Strada del Drosso, 183
P3	Piazzale Gorizia, 212a
P4	Via Issiglio, 36
P5	Corso Marche, 5

Table 3. Identification codes and locations of the selected piezometers.

Figure 13. illustrates the spatial distribution of the selected piezometers across the municipal area of Turin.

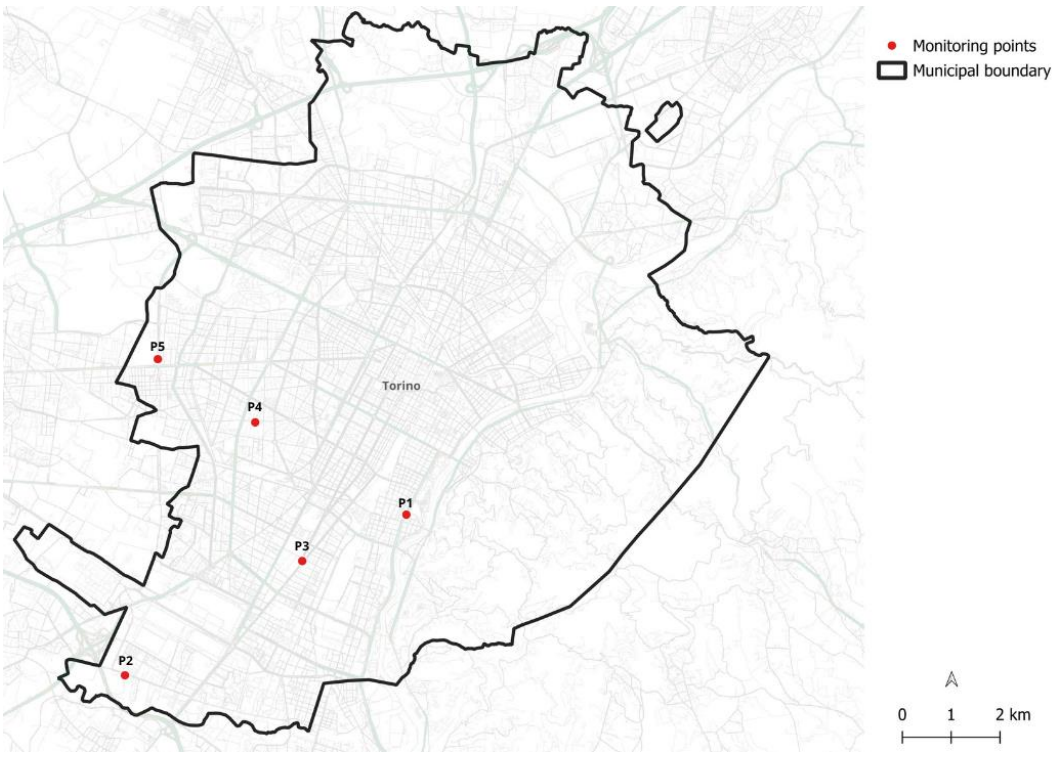


Figure 13. Spatial distribution and location information of the selected piezometers within the municipal boundary of Turin. Elaborated by the author using the piezometer location dataset, municipal boundary data, and OpenStreetMap base map.

1. **Piezometer 1 – Corso Massimo D 'Azeglio, 21**

- Location and urban context

Piezometer 1 is located in the south-eastern part of Turin along Corso Massimo D'Azeglio, near the Po River and Parco del Valentino. The site represents a transitional urban context, characterized by dense built-up areas on the western side and large green and permeable surfaces associated with the river corridor on the eastern side.

Figure 14 shows the location of Piezometer 1 within the municipal boundary of Turin and highlights its position near the Po River and Parco del Valentino, providing spatial context for the surrounding urban environment. (Piezometer 1 has a depth of approximately 25 m).

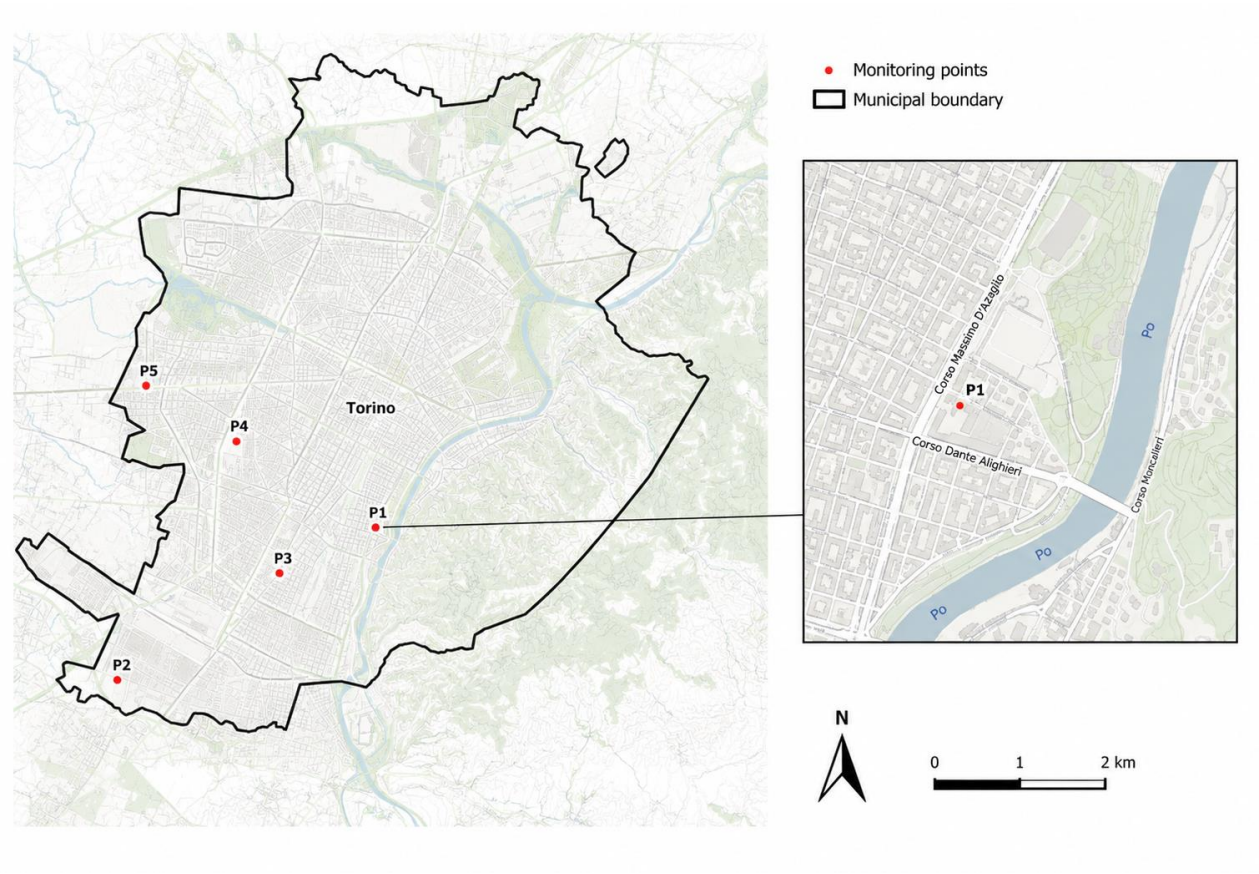


Figure 14. Location of Piezometer 1 within the municipal boundary of Turin. Elaborated by the author using the piezometer location dataset, municipal boundary data, and OpenStreetMap base map.

- **Land use analysis**

The area surrounding Piezometer 1 is primarily composed of dense and low-density residential zones within the 200 m buffer. Smaller sections include industrial/commercial areas and road infrastructure, contributing to a mixed urban land-use context.

Green and recreational areas are concentrated in the eastern part of the buffer, near Parco del Valentino and the Po River corridor. Although limited in size, these areas provide localized permeable and vegetated surfaces within the surrounding built environment.

Figure 15 shows the land-use classification within the 200 m buffer area around Piezometer 1.

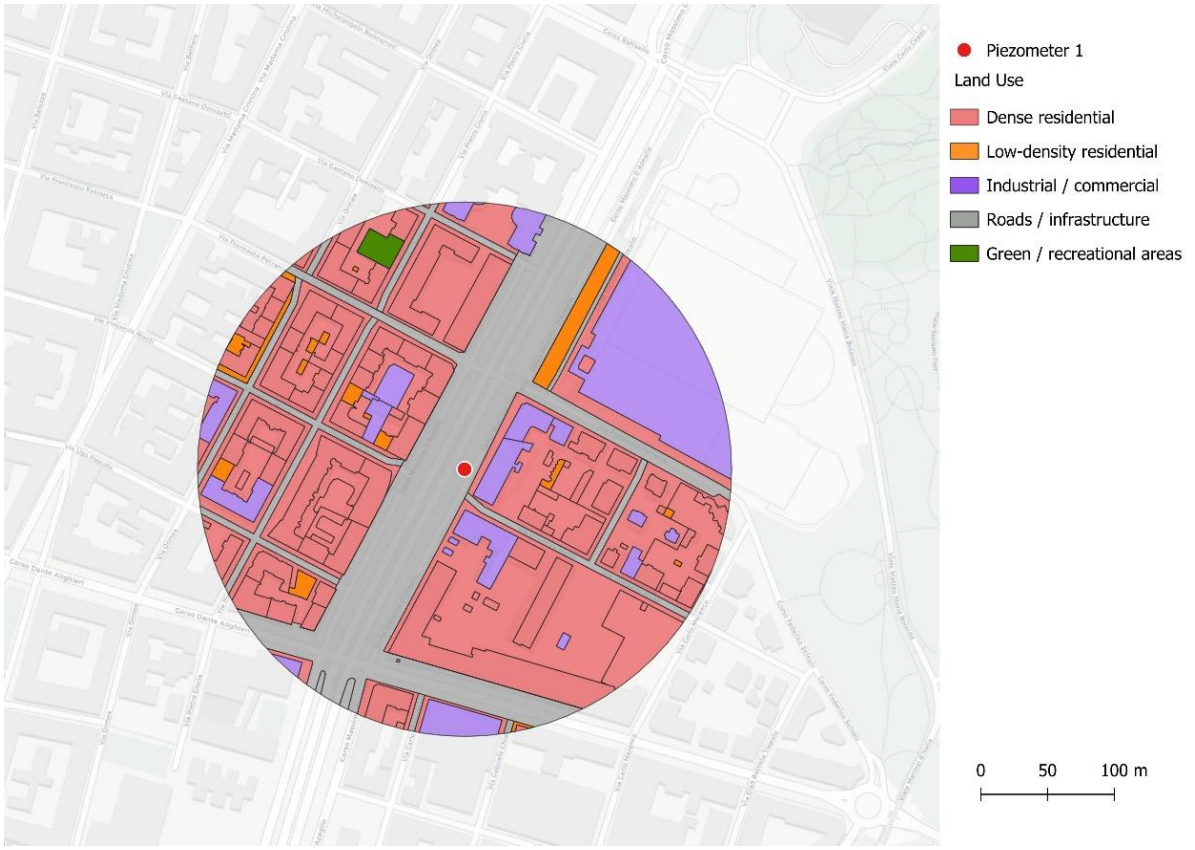


Figure 15. Land-use classification within the 200 m buffer area surrounding Piezometer 1. Elaborated by the author using GIS analysis of the land-use dataset described in Chapter 3.

- **Building Height Analysis**

Analysis of building-height classes within the 200 m buffer shows that the area surrounding Piezometer 1 is mainly composed of low- to medium-rise buildings. Buildings with 2–3 floors and 4–7 floors are dominant, while some taller structures in the 8–18 floor class are also present. This pattern indicates a compact urban fabric with moderate vertical development rather than a predominantly high-rise environment.

Figure 16 shows the building-height classification within the 200 m buffer area around Piezometer 1.

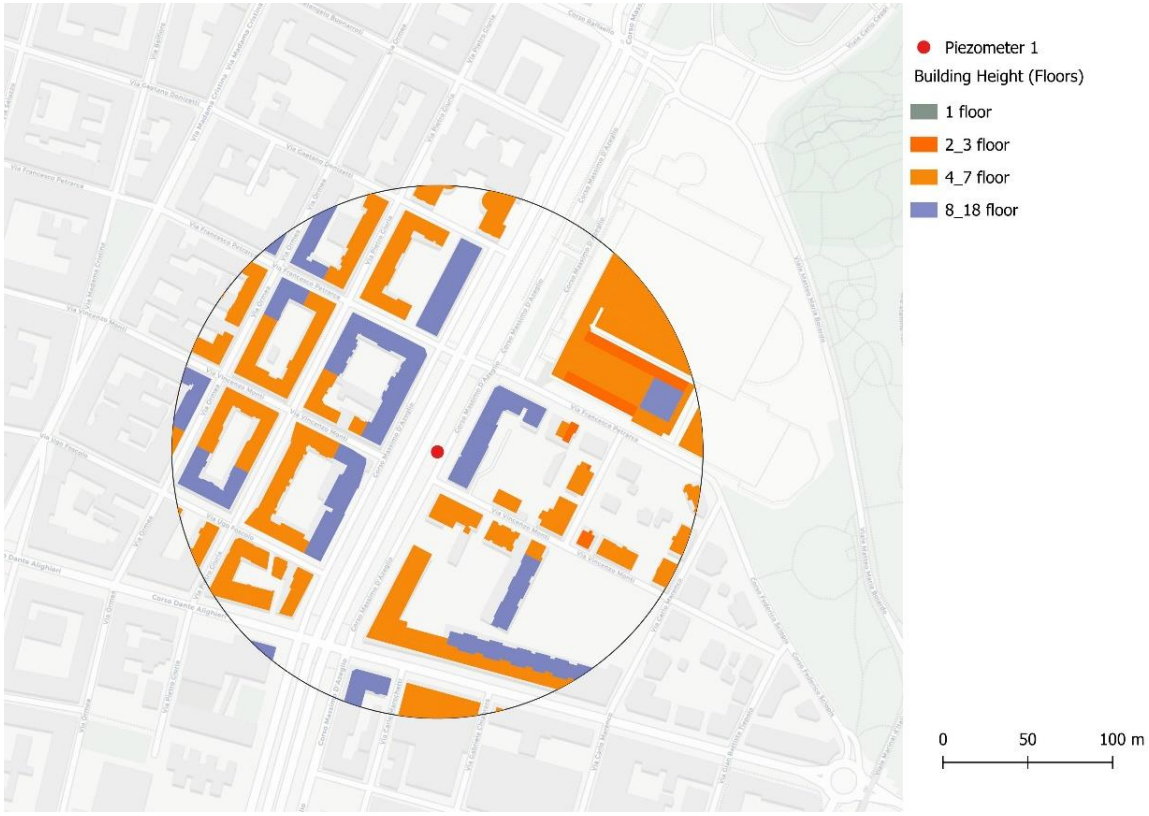


Figure 16. Building-height classification within the 200 m buffer area surrounding Piezometer 1. Elaborated by the author using GIS analysis of the building-height dataset described in Chapter 3.

Piezometer 2 – Strada del Drosso, 183

- Location and urban context

Piezometer 2 is located in the south-western part of Turin along Strada del Drosso. The surrounding area is characterized by industrial and commercial land uses, including factories, warehouses, transport infrastructure, and paved surfaces. Compared with Piezometer 1, the site represents a less compact urban context, with a mixture of built-up areas and open or less densely developed surfaces.

Figure 17 shows the location of Piezometer 2 within the municipal boundary of Turin and provides a detailed view of its surrounding urban context (Piezometer 2 has a depth of approximately 28 m).

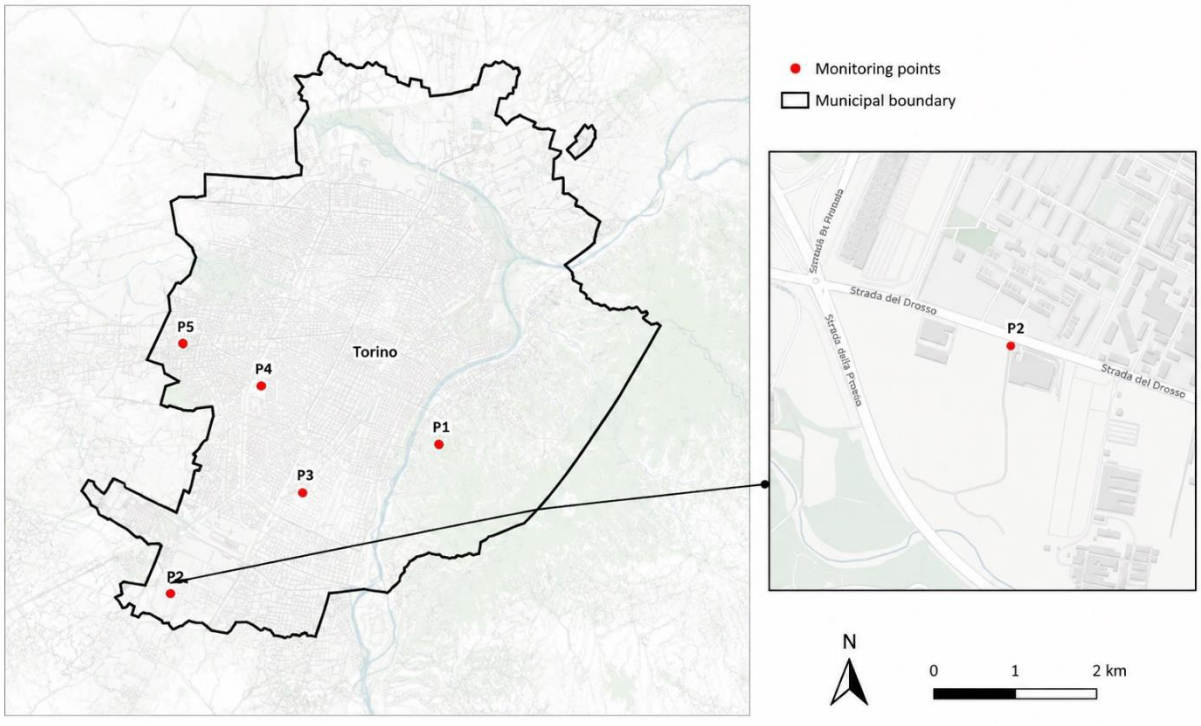


Figure 17. Location of Piezometer 2 within the municipal boundary of Turin. Elaborated by the author using the piezometer location dataset, municipal boundary data, and OpenStreetMap base map.

.

- **Land use analysis**

Within the 200 m buffer around Piezometer 2, the area is characterized by a mixed land-use pattern, including residential, industrial/commercial, transport infrastructure, and open or agricultural land. Dense residential areas are mainly located in the northern part of the buffer, while industrial and commercial uses are concentrated near the monitoring point and along the nearby transport corridor. Roads and transport infrastructure cross the buffer area, contributing to the presence of sealed surfaces.

The southern part of the buffer includes non-irrigated agricultural land and other vegetated areas, which provide permeable surfaces within an otherwise partially built-up environment. Urban green areas are limited and appear only in small portions of the buffer.

Figure 18 shows the land-use classification within the 200 m buffer area surrounding Piezometer 2.



Figure 18. Land-use classification within the 200 m buffer area surrounding Piezometer 2. Elaborated by the author using GIS analysis of the land-use dataset described in Chapter 3.

- **Building Height Analysis**

The area surrounding Piezometer 2 is characterized by relatively low building coverage and a discontinuous built-up pattern. Within the 200 m buffer, the classified buildings are mainly located in the northern part of the area, close to Strada del Drosso. Although the number of buildings is limited, several of them fall within the 8–18 floor class, while fewer structures are classified within the 4–7 floor and 2–3 floor ranges.

The immediate surroundings of the monitoring point include industrial/commercial facilities, transport infrastructure, and open or agricultural land, resulting in a less continuous urban fabric compared with Piezometer 1. This pattern indicates a mixed peripheral context, where built structures are present but are separated by larger open spaces and less densely developed surfaces.

Figure 19 shows the building-height classification within the 200 m buffer area surrounding Piezometer 2.

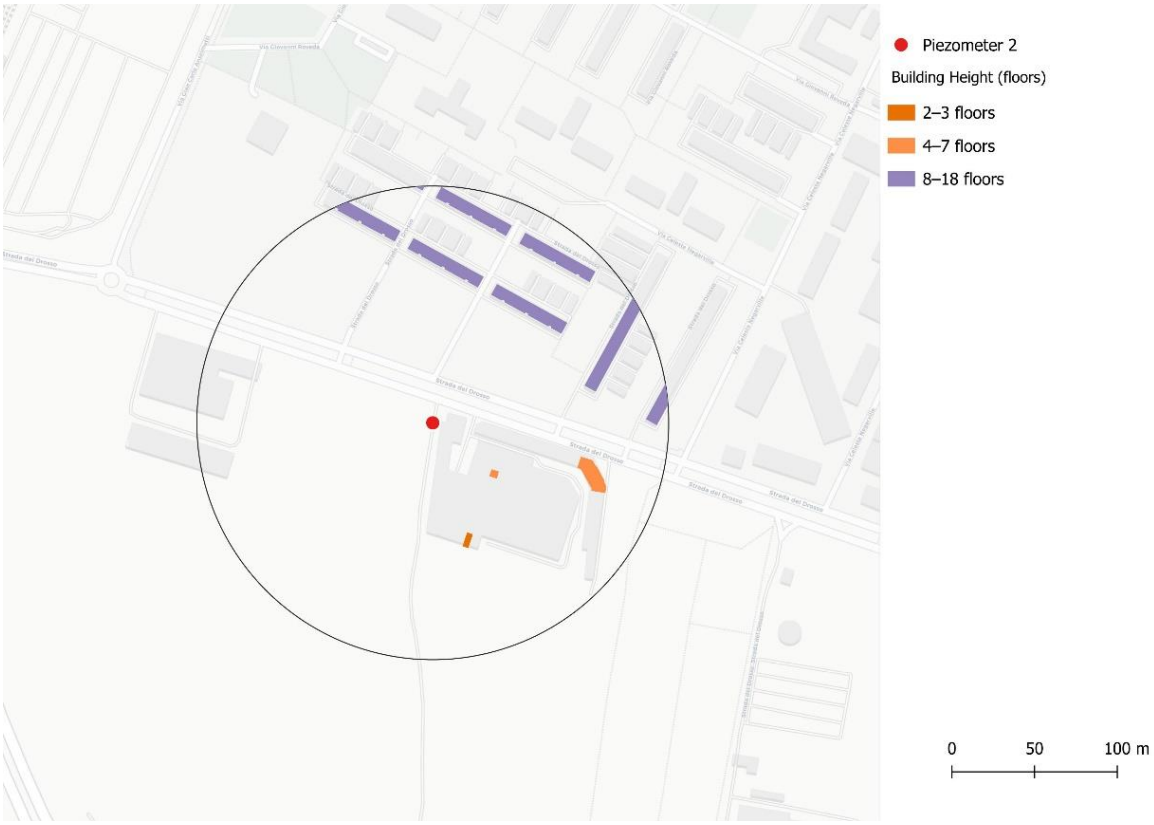


Figure 19. Building-height classification within the 200 m buffer area surrounding Piezometer 2. Elaborated by the author using GIS analysis of the building-height dataset described in Chapter 3.

Piezometer 3 – Piazzale Gorizia, 212a

- Location and urban context

Piezometer 3 is located in the south-central part of Turin, close to the intersection of Corso Unione Sovietica and Via Filadelfia, near the Stadio Olimpico Grande Torino and nearby sports facilities. The site is situated in a densely built-up urban area characterized by residential buildings, public facilities, shops, and major road infrastructure. The surrounding area is largely covered by roads, buildings, and other urban surfaces, with limited open or permeable ground.

Figure 20 shows the location of Piezometer 3 within the municipal boundary of Turin and provides a detailed view of its surrounding urban context (Piezometer 3 has a depth of approximately 26.5 m).

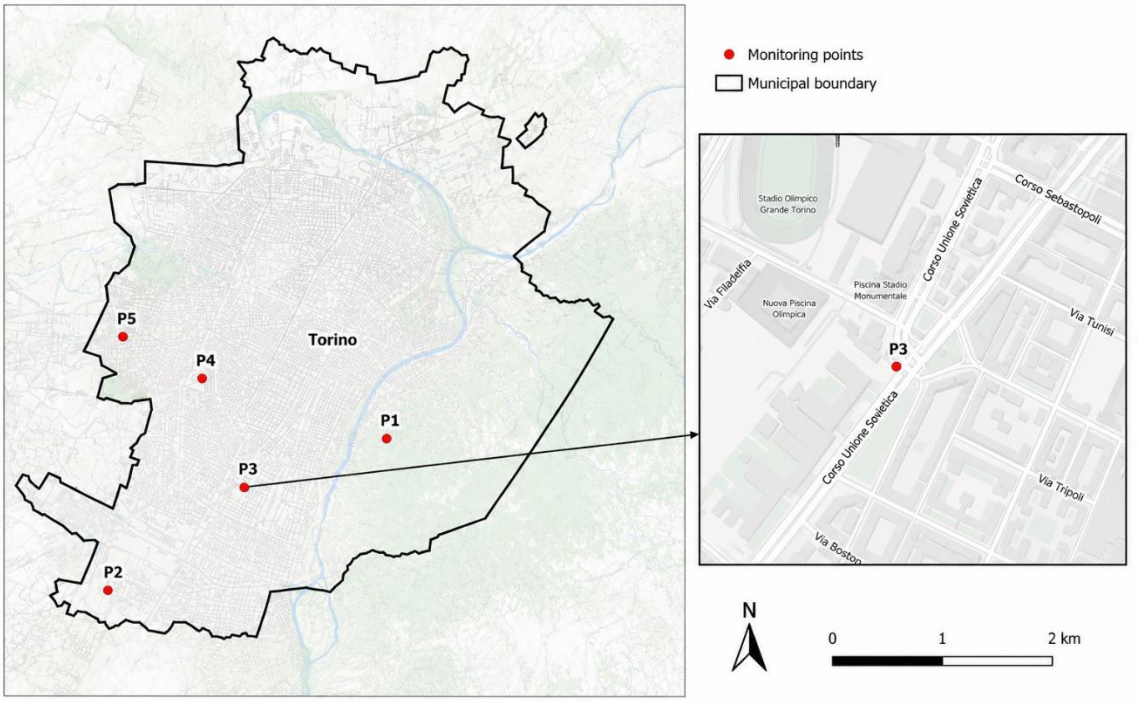


Figure 20. Location of Piezometer 3 within the municipal boundary of Turin. Elaborated by the author using the piezometer location dataset, municipal boundary data, and OpenStreetMap base map.

- **Land use analysis**

The area surrounding Piezometer 3 is predominantly urbanized. Within the 200 m buffer, dense residential areas represent the main land-use category, reflecting the compact urban fabric typical of this part of Turin. Industrial/commercial areas are also present, especially to the west of the monitoring point, while roads and transport infrastructure occupy a substantial portion of the buffer, mainly along Corso Unione Sovietica.

Urban green areas and other vegetated spaces are scattered within the buffer, particularly near sports and recreational facilities. Compared with Piezometer 2, the area around Piezometer 3 shows a more compact and continuous built-up structure, with a higher presence of residential buildings, paved surfaces, and transport infrastructure. The land-use configuration characterizes the surroundings of Piezometer 3 as a compact urban context, with a combination of dense residential development, transport infrastructure, paved surfaces, and limited open or vegetated areas..

Figure 21 shows the land-use classification within the 200 m buffer area surrounding Piezometer 3.



Figure 21. Land-use classification within the 200 m buffer area surrounding Piezometer 3. Elaborated by the author using GIS analysis of the land-use dataset described in Chapter 3.

- **Building Height Analysis**

The building-height classification within the 200 m buffer around Piezometer 3 shows a predominance of medium- to high-rise buildings. Most classified buildings fall within the 4–7 floor and 8–18 floor classes. Buildings with 8–18 floors are mainly located along the main urban corridors and within residential blocks, while 4–7 floor buildings are more evenly distributed throughout the surrounding area.

Very low-rise buildings are limited within the buffer, indicating a relatively dense and vertically developed urban fabric. The area includes residential, commercial, and institutional functions, together with major road infrastructure and paved surfaces. Compared with Piezometer 2, the surroundings of Piezometer 3 present a more compact and continuous built-up structure.

Figure 22 shows the building-height classification within the 200 m buffer area surrounding Piezometer 3.

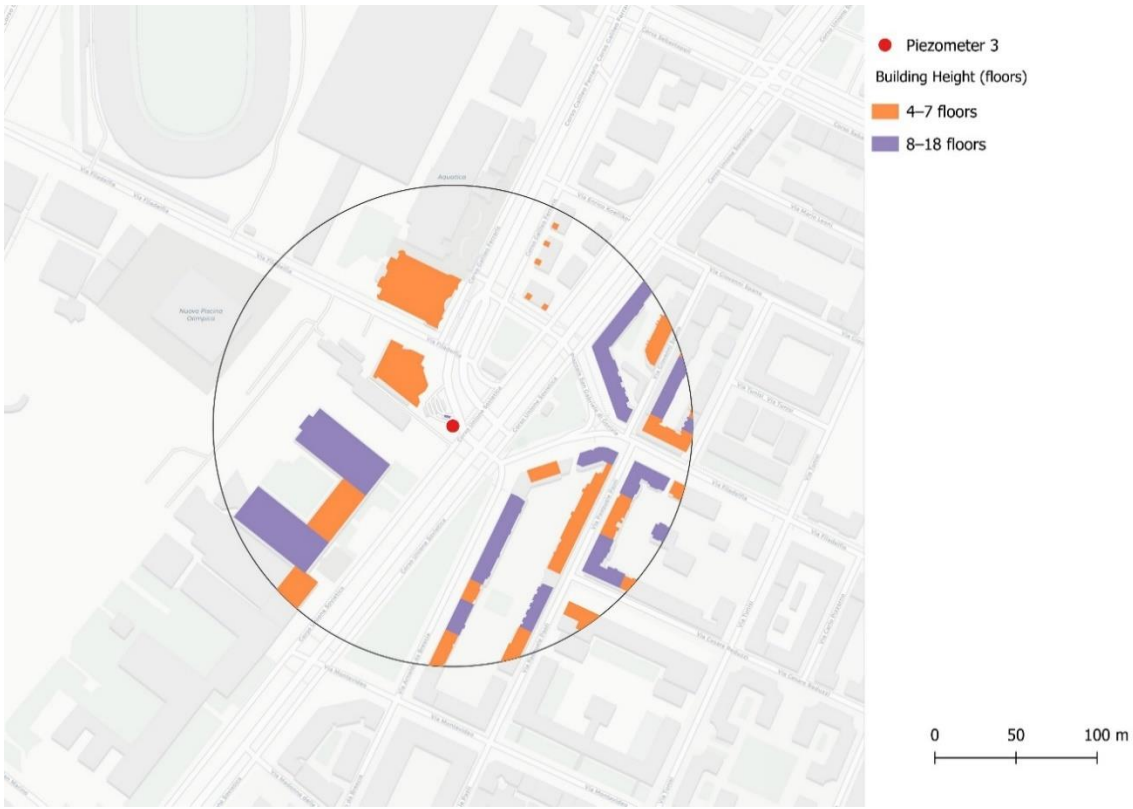


Figure 22. Building-height classification within the 200 m buffer area surrounding Piezometer 3. Elaborated by the author using GIS analysis of the building-height dataset described in Chapter 3

Piezometer 4 – Via Issiglio, 36

- Location and urban context

Piezometer 4 is located in the western part of Turin, close to Via Issiglio and Corso Trapani, within a consolidated residential urban area. The surrounding context is characterized by a continuous built-up fabric, with a strong presence of apartment buildings, paved surfaces, and limited open or permeable areas. The area therefore represents a dense residential urban setting characterized by continuous development and limited open space.

Figure 23 shows the location of Piezometer 4 within the municipal boundary of Turin and provides a detailed view of its surrounding urban context. (Piezometer 4 has a depth of approximately 36 m).

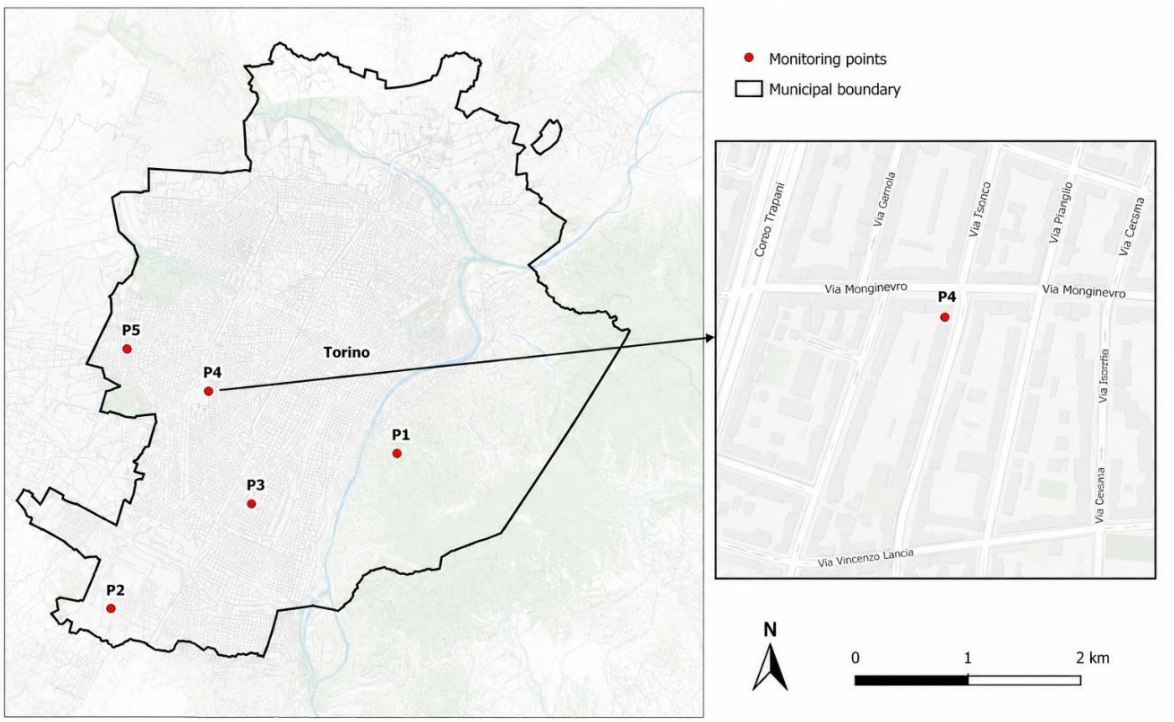


Figure 23. Location of Piezometer 4 within the municipal boundary of Turin. Elaborated by the author using the piezometer location dataset, municipal boundary data, and OpenStreetMap base map.

- **Land use analysis**

The area surrounding Piezometer 4 is predominantly characterized by dense residential land use within the 200 m buffer. The neighbourhood consists mainly of compact residential blocks, which are typical of the western urban districts of Turin. Low-density residential areas are also present, with isolated buildings and small courtyards distributed within the buffer.
Industrial/commercial areas occupy only limited portions of the buffer and are less extensive than the residential land uses. Roads and transport infrastructure, particularly the main east–west corridor crossing the area, represent an important component of the local land-use pattern and contribute to surface sealing. Urban green areas are very limited, indicating a low presence of permeable and vegetated surfaces around the monitoring point.

Figure 24 shows the land-use classification within the 200 m buffer area surrounding Piezometer 4.

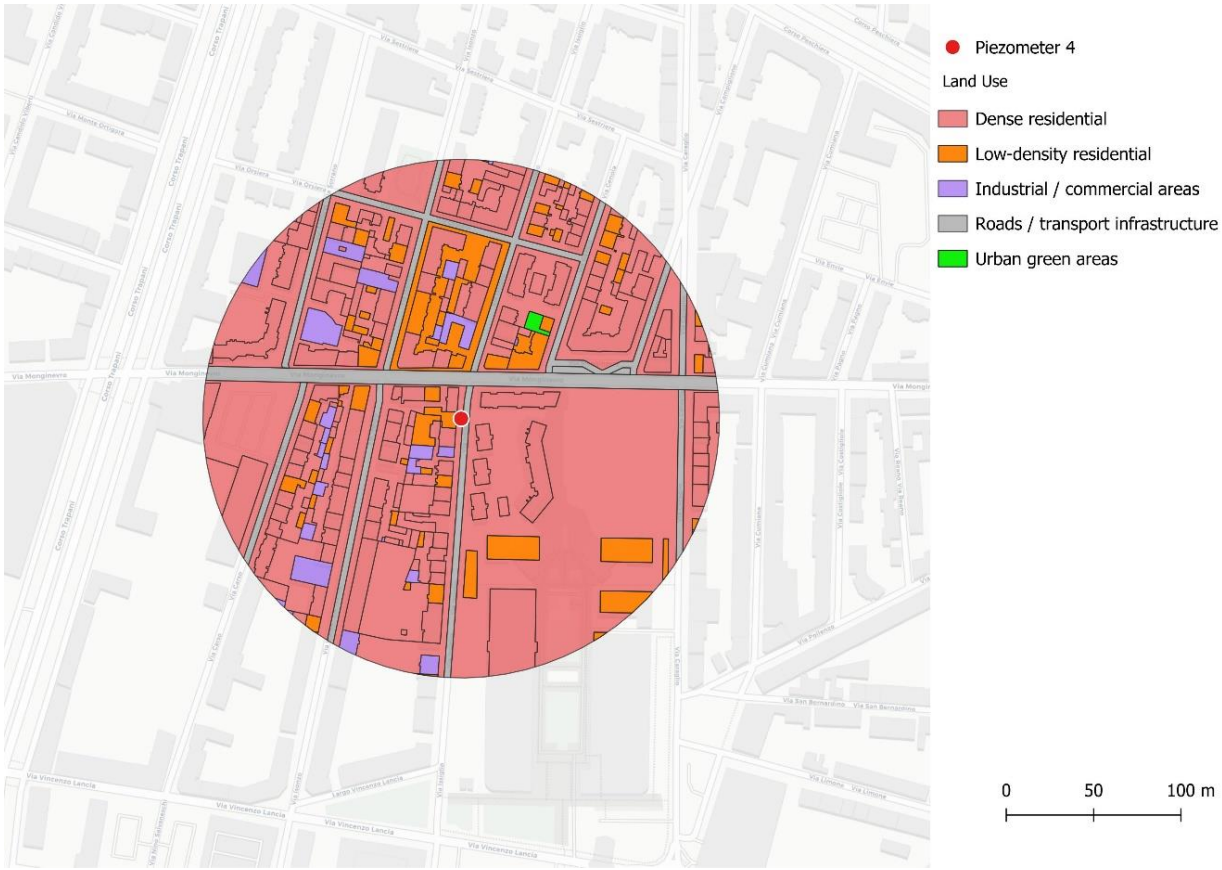


Figure 24. Land-use classification within the 200 m buffer area surrounding Piezometer 4. Elaborated by the author using GIS analysis of the land-use dataset described in Chapter 3.

- **Building Height Analysis**

Most buildings around Piezometer 4 are medium-rise residential structures, mainly within the 4–7 floor class. These buildings form a dense and continuous urban fabric, which is typical of established residential neighborhoods in the western part of Turin. The 4–7 floor buildings are widely distributed throughout the buffer area and represent the dominant building-height class around the monitoring point.

A smaller number of buildings fall within the 8–18 floor class, mostly located in specific residential blocks or larger building complexes. Very low-rise and very high-rise buildings are almost absent, indicating a relatively homogeneous urban fabric dominated by moderate building heights.

Figure 25 shows the building-height classification within the 200 m buffer area surrounding Piezometer 4.



Figure 25. Building-height classification within the 200 m buffer area surrounding Piezometer 4. Elaborated by the author using GIS analysis of the building-height dataset described in Chapter 3.

Piezometer 5 – Corso Marche, 5

- Location and urban context

Piezometer 5 is located in the north-western part of Turin, close to the intersection between Corso Marche and Corso Francia. The site is situated within a consolidated urban area characterized by major road infrastructure, residential buildings, and large built-up blocks. The surrounding context represents a mixed urban setting characterized by major transport corridors, paved surfaces, residential buildings, and large built-up blocks.

Figure 26 shows the location of Piezometer 5 within the municipal boundary of Turin and provides a detailed view of its surrounding urban context (Piezometer 5 has a depth of approximately 41.5 m).

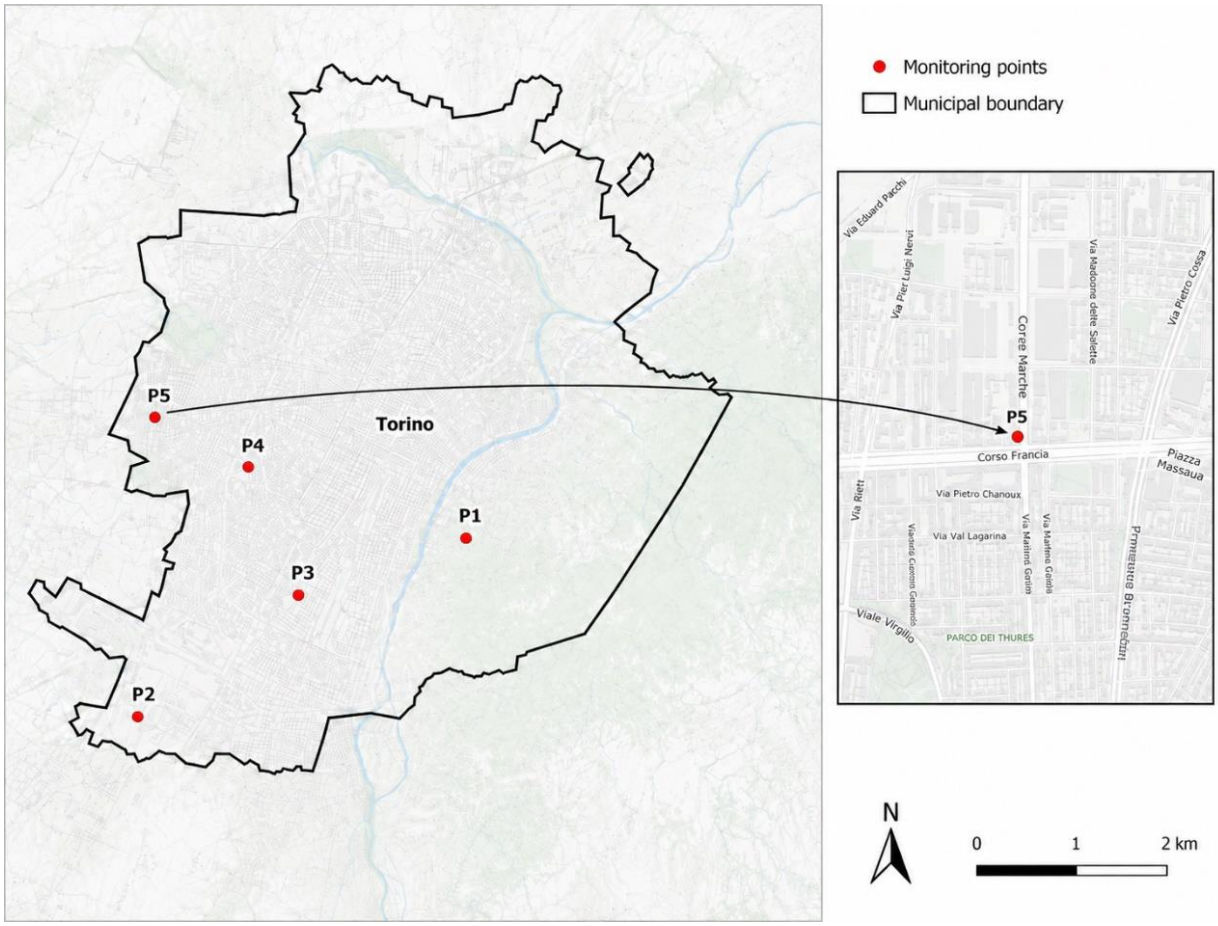


Figure 26. Location of Piezometer 5 within the municipal boundary of Turin. Elaborated by the author using the piezometer location dataset, municipal boundary data, and OpenStreetMap base map.

- **Land use analysis**

Within the 200 m buffer around Piezometer 5, the area is characterized by a mixed urban land-use pattern. The western part of the buffer is mainly occupied by industrial/commercial areas, while the eastern part includes dense and low-density residential land uses. Corso Marche and Corso Francia represent major transport corridors crossing the area and contribute to the presence of sealed surfaces and road infrastructure.

Small urban green areas are also present, mainly in the eastern part of the buffer. Overall, the site combines residential, industrial/commercial, transport, and limited green areas within a compact urban setting. This land-use configuration characterizes Piezometer 5 as a mixed urban context combining residential, industrial/commercial, transport, and limited green areas within the 200 m buffer..

Figure 27 shows the land-use classification within the 200 m buffer area surrounding Piezometer 5.



Figure 27. Land-use classification within the 200 m buffer area surrounding Piezometer 5. Elaborated by the author using GIS analysis of the land-use dataset described in Chapter 3.

- **Building Height Analysis**

The building-height classification within the 200 m buffer around Piezometer 5 shows a mixed pattern of medium-rise and taller buildings. Most classified buildings fall within the 4–7 floor class, while several 8–18 floor buildings are also present, mainly in the eastern and southern parts of the buffer. This indicates a medium- to high-density built environment associated with both residential and commercial functions.

Although some large industrial/commercial plots and open spaces are present, the surrounding area remains strongly influenced by built structures, paved surfaces, and major transport corridors.

Figure 28 shows the building-height classification within the 200 m buffer area surrounding Piezometer 5.



Figure 28. Building-height classification within the 200 m buffer area surrounding Piezometer 5. Elaborated by the author using GIS analysis of the building-height dataset described in Chapter 3.

.

3.3 Assumptions and Limitations

✓ Assumptions

- Groundwater temperature measurements obtained from the five monitoring piezometers are representative of local groundwater conditions.
- The selected buffer area around each monitoring point adequately represents the surrounding urban environment.
- Land-use and building-height datasets provide a reliable description of the urban characteristics surrounding the monitoring points.
- Climatic observations available for Turin are considered representative of the general meteorological conditions during the monitoring period.
- Urban land-use patterns remained substantially stable during the study period.

✓ Limitations

- The study is based on data from only five monitoring piezometers.
- P1 had a shorter monitoring period due to sensor problems, which limited comparison with the other piezometers.
- Spatial variability of groundwater temperature may not be fully captured by the selected monitoring network.
- Direct measurements of groundwater flow, recharge rates, and subsurface thermal properties were not available.
- The influence of individual underground infrastructures, geothermal systems, and local anthropogenic heat sources was not explicitly quantified.
- The results are specific to the monitored locations and to the hydrogeological and urban context of Turin and should not be generalized to the entire city without additional monitoring data.

Chapter 4 – Results

4.1 Spatial and temporal patterns of groundwater temperature in Turin

4.1.1 Monitoring periods, data availability, and quality control

Groundwater temperature data were collected from five selected piezometers located within the municipal area of Turin. This section provides a general overview of the monitoring periods and the number of valid temperature measurements available for each piezometer before presenting the descriptive and temporal analyses. The monitoring duration was not identical at all sites, mainly because of differences in sensor operation and data availability.

Before the statistical analysis, the temperature records were checked for possible sensor-handling events. Periods associated with sensor removal, reinsertion, or immediate post-reinsertion stabilization were excluded. Where pressure records were available, sudden pressure changes occurring together with abrupt temperature variations were used as an additional indicator of possible sensor disturbance. Only measurements considered representative of normal groundwater-monitoring conditions were retained for the subsequent analyses.

P1 has the shortest monitoring period, extending from 11 December 2024 to 27 May 2025, due to sensor-related limitations. P2, P4, and P5 have longer and comparable monitoring periods, extending from 29 October 2024 to 4 May 2026, while P3 was monitored from 29 October 2024 to 13 March 2026. Despite its slightly shorter monitoring period compared with P2, P4, and P5, P3 contains the largest number of valid temperature measurements. Differences in the number of observations reflect both the monitoring duration and the continuity of the available records.

Table 4 summarizes the monitoring start and end dates and the number of valid groundwater temperature measurements retained for each piezometer after data quality control. These differences in monitoring duration and data availability should be considered when interpreting the subsequent statistical and temporal analyses, particularly when directly comparing temperature variability among the monitoring points.

Piezometer	Monitoring start	Monitoring end	Number of valid temperature measurements
P1	11 December 2024	27 May 2025	14101
P2	29 October 2024	4 May 2026	52965
P3	29 October 2024	13 March 2026	71970
P4	29 October 2024	4 May 2026	52960
P5	29 October 2024	4 May 2026	52966

Table 4.Monitoring period and number of groundwater temperature measurements for the selected piezometers, compiled by the author from the groundwater monitoring dataset used in this study.

4.1.2 Descriptive statistics of groundwater temperature

Table 5 presents the main descriptive statistics of groundwater temperature for the five piezometers, including mean, median, minimum, maximum, and standard deviation values, allowing comparison of temperature levels and variability among the monitoring points. In detail, P3 recorded the highest mean groundwater temperature, with an average value of 17.33 °C and a median of 17.46 °C. The minimum and maximum temperatures at this piezometer were 16.58 °C and 17.86 °C, respectively, while the standard deviation was 0.39 °C, indicating the highest temperature variability among the five monitoring points. P1 showed the second-highest mean temperature, at 16.15 °C, with a median of 16.13 °C. Its temperature ranged from a minimum of 15.98 °C to a maximum of 16.26 °C, with a standard deviation of 0.05 °C. P4 recorded a mean temperature of 14.49 °C and a median of 14.48 °C, with minimum and maximum values of 14.44 °C and 14.56 °C, respectively, and a standard deviation of 0.02 °C. P2 had a mean and median temperature of 14.23 °C, with temperatures ranging from 14.19 °C to 14.27 °C and a standard deviation of 0.01 °C, representing the lowest variability among the monitored piezometers. Finally, P5 recorded the lowest mean groundwater temperature, at 13.95 °C, with the same median value of 13.95 °C. Its minimum and maximum temperatures were 13.82 °C and 15.41 °C, respectively, with a standard deviation of 0.08 °C. Overall, P3 showed the highest mean groundwater temperature and the greatest temporal variability among the five monitoring points. In contrast, P1, P2, P4, and P5 showed comparatively limited temperature variability over their respective monitoring periods, although the shorter record available for P1 should be considered when making direct comparisons.

Piezometer	Mean (°C)	Median (°C)	Minimum (°C)	Maximum (°C)	Standard deviation (°C)
P1	16.15	16.13	15.98	16.26	0.05
P2	14.23	14.23	14.19	14.27	0.01
P3	17.33	17.46	16.58	17.86	0.39
P4	14.49	14.48	14.44	14.56	0.02
P5	13.95	13.95	13.82	15.41	0.08

Table 5.Descriptive statistics of groundwater temperature at the five piezometers, calculated by the author from the groundwater temperature dataset used in this study.

Month	P1 (°C)	P2 (°C)	P3 (°C)	P4 (°C)	P5 (°C)
24-Oct		14.37	17.16	14.55	14.02
24-Nov		14.22	17.31	14.47	13.97
24-Dec	16.16	14.22	17.61	14.46	13.96
25-Jan	16.18	14.22	17.73	14.46	13.95
25-Feb	16.13	14.22	17.70	14.46	13.95
25-Mar	16.14	14.22	17.57	14.46	13.99
25-Apr	16.13	14.22	17.43	14.47	13.97
25-May	16.12	14.24	17.16	14.48	13.98
25-Jun		14.23	16.91	14.47	13.94
25-Jul		14.25	16.79	14.48	13.98
25-Aug		14.25	16.61	14.47	13.99
25-Sep		14.24	16.72	14.48	13.98
25-Oct		14.24	17.06	14.48	13.94
25-Nov		14.23	17.46	14.50	13.93
25-Dec		14.22	17.74	14.51	13.93
26-Jan		14.22	17.82	14.51	13.90
26-Feb		14.22	17.72	14.52	13.89
26-Mar		14.22	17.58	14.53	13.88
26-Apr		14.23		14.54	13.89
26-May		14.23		14.54	13.84

Table 6.Monthly mean groundwater temperature at the five piezometers, calculated by the author from the groundwater temperature dataset used in this study.

P3 showed a distinct temporal pattern, with groundwater temperature decreasing from winter toward summer, reaching its lowest monthly mean in August 2025 (16.61 °C), and subsequently increasing again to a maximum of 17.82 °C in January 2026. This behavior differs clearly from the comparatively stable patterns observed at the other monitoring points and is examined in greater detail in the Discussion.

The temporal patterns described above are further illustrated in Figure 29, which shows the monthly mean groundwater temperature trends for the five monitoring points. The figure highlights the relatively stable temperatures observed at P1, P2, P4, and P5, as well as the more pronounced seasonal variation recorded at P3.

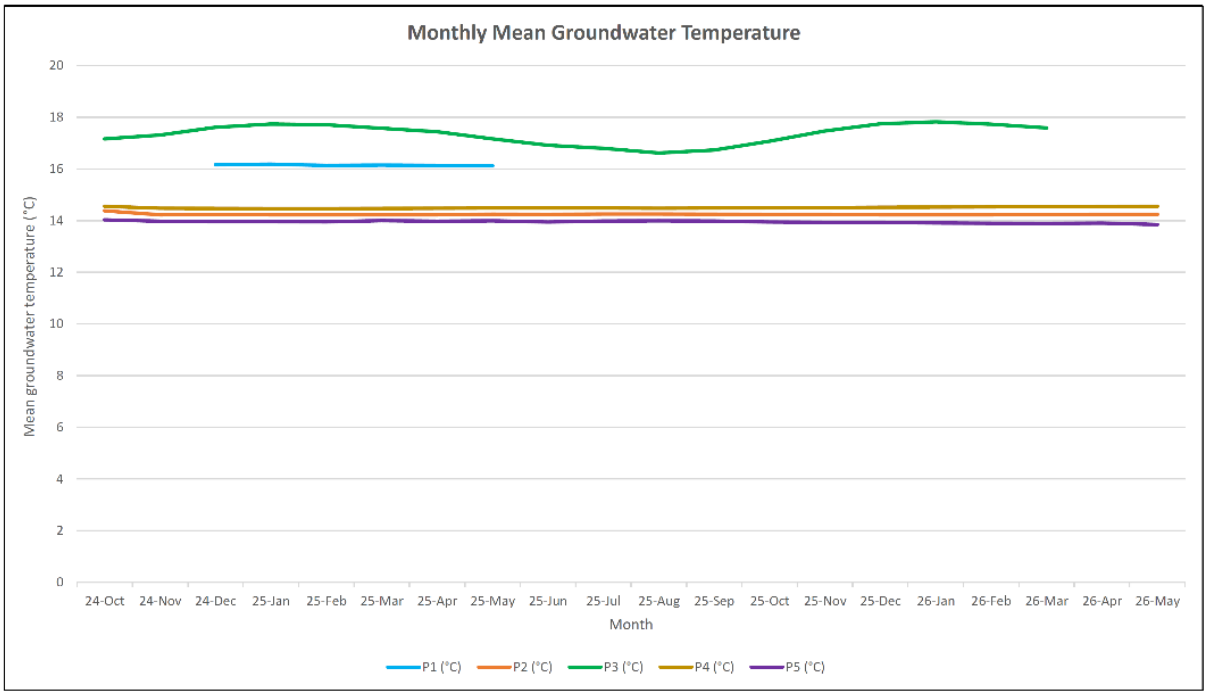


Figure 29. Monthly mean groundwater temperature trends at the five piezometers, calculated by the author from the groundwater temperature dataset used in this study.

4.1.3 Detailed temporal analysis of P3 and meteorological conditions

Given the distinct temporal behavior observed at P3, a more detailed analysis was conducted to examine its relationship with precipitation. The analysis used the final quality-controlled P3 dataset, containing 71,970 valid observations, together with precipitation data from the ARPA Piemonte Torino Via della Consolata meteorological station. The common period available for the two datasets extended from 29 October 2024 to 28 October 2025, providing 366 days of overlapping daily data. During this period, total precipitation was 689.4 mm, distributed over 95 rainy days.

For the correlation analysis, precipitation was aggregated to daily totals and P3 groundwater temperature was represented by daily mean values. Both contemporaneous and lagged relationships

were evaluated. Positive lag values indicate that precipitation occurred on day t, while groundwater temperature or daily temperature change was evaluated on day t + lag.

No significant contemporaneous relationship was observed between daily precipitation and the absolute groundwater temperature at P3 (Pearson $r = -0.020$, $p = 0.706$; Spearman $\rho = 0.020$, $p = 0.701$; $N = 366$). Similarly, correlations between precipitation and subsequent absolute groundwater temperature remained negligible across lags from 0 to 30 days, and no statistically robust lagged relationship was identified after correction for multiple testing.

A different pattern was observed when daily changes in P3 groundwater temperature were considered. The contemporaneous Pearson correlation was negligible ($r = -0.040$, $p = 0.446$), whereas a weak negative Spearman correlation was detected ($\rho = -0.166$, $p = 0.00145$). Lagged analysis showed a clearer negative association approximately 7–11 days after precipitation. The strongest Pearson correlation occurred at a lag of 10 days ($r = -0.201$, $p = 0.000132$, FDR-adjusted $q = 0.00374$), while the largest Spearman coefficient occurred at a lag of 8 days ($\rho = -0.270$, $p = 2.18 \times 10^{-7}$, FDR-adjusted $q = 4.45 \times 10^{-6}$). Although statistically detectable, these associations were weak; The squared Pearson correlation at the 10-day lag was approximately 0.041, indicating that the linear association accounted for about 4% of the variance in daily temperature change.

A complementary rainfall-event analysis was performed for 25 precipitation events with total rainfall of at least 5 mm, ranging from 5.4 to 83.7 mm. P3 temperature changes were calculated relative to the mean groundwater temperature during the six hours preceding each event. Mean temperature change was small immediately after rainfall (−0.003 °C after one day) and became progressively more negative with time, reaching −0.019 °C after 7 days, −0.032 °C after 10 days, and −0.048 °C after 14 days. The corresponding median changes were −0.023 °C, −0.036 °C, and −0.058 °C, respectively. Although nominal p-values below 0.05 were obtained for some of the later response windows, none of the event-based comparisons remained statistically significant after correction for multiple testing (minimum adjusted $q = 0.156$).

Overall, the analysis identified no detectable immediate association between precipitation and absolute P3 groundwater temperature. A weak but statistically detectable negative association was observed between precipitation and subsequent daily temperature changes, with the clearest lagged signal occurring approximately 8–10 days after rainfall. The event-based analysis showed a similar gradual negative temperature tendency, although these event-level differences were not statistically significant after multiple-testing correction. Table 7 shows that the strongest delayed associations occurred approximately 8–10 days after precipitation. The maximum Pearson correlation was observed at 10 days ($r = -0.201$), while the strongest Spearman correlation occurred at 8 days ($\rho = -0.270$). Both relationships were weak in magnitude.

Lag (days)	N	Pearson r	Pearson FDR q	Spearman ρ	Spearman FDR q
7	359	−0.111	0.101	−0.248	1.51×10^{-5}
8	358	−0.139	0.0514	**−0.270**	**4.45×10^{-6}**
9	357	−0.193	0.00374	−0.254	1.17×10^{-5}
10	356	**−0.201**	**0.00374**	−0.268	**4.45×10^{-6}**
11	355	−0.187	0.00422	−0.241	2.63×10^{-5}

Table 7.Selected lagged correlations between daily precipitation and subsequent daily changes in P3 groundwater temperature.

Positive lag indicates that P3 temperature change was evaluated the specified number of days after precipitation. FDR q-values refer to multiple-testing-adjusted significance levels.

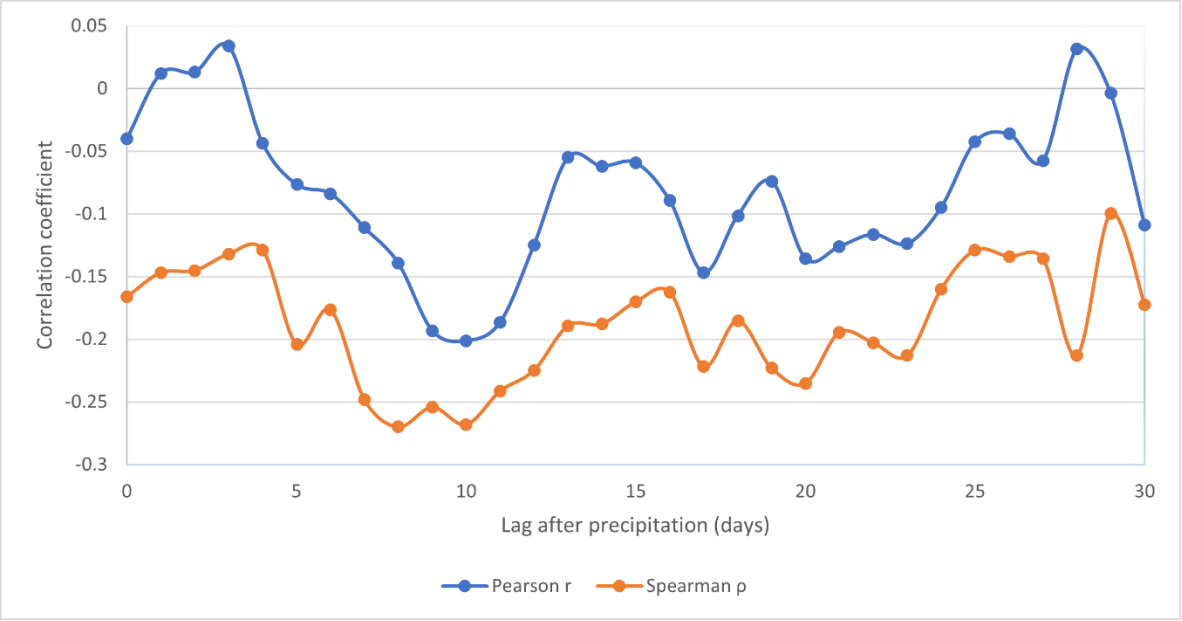


Figure 30. Lagged Pearson and Spearman correlations between daily precipitation and subsequent daily changes in P3 groundwater temperature over lags of 0–30 days. Positive lag indicates that temperature change was evaluated after the corresponding precipitation day. Elaborated by the author.

As shown in Figure 30, the clearest negative lagged association occurred approximately 8–10 days after precipitation. The strongest Pearson correlation was observed at a lag of 10 days ($r = -0.201$), while the strongest Spearman correlation occurred at a lag of 8 days ($\rho = -0.270$).

Figure 31 shows an almost negligible temperature change immediately after rainfall, followed by a gradual decrease over the subsequent days. Mean ΔT decreased from −0.003 °C after one day to −0.032 °C after 10 days and −0.048 °C after 14 days. However, the event-based differences did not remain statistically significant after correction for multiple testing.

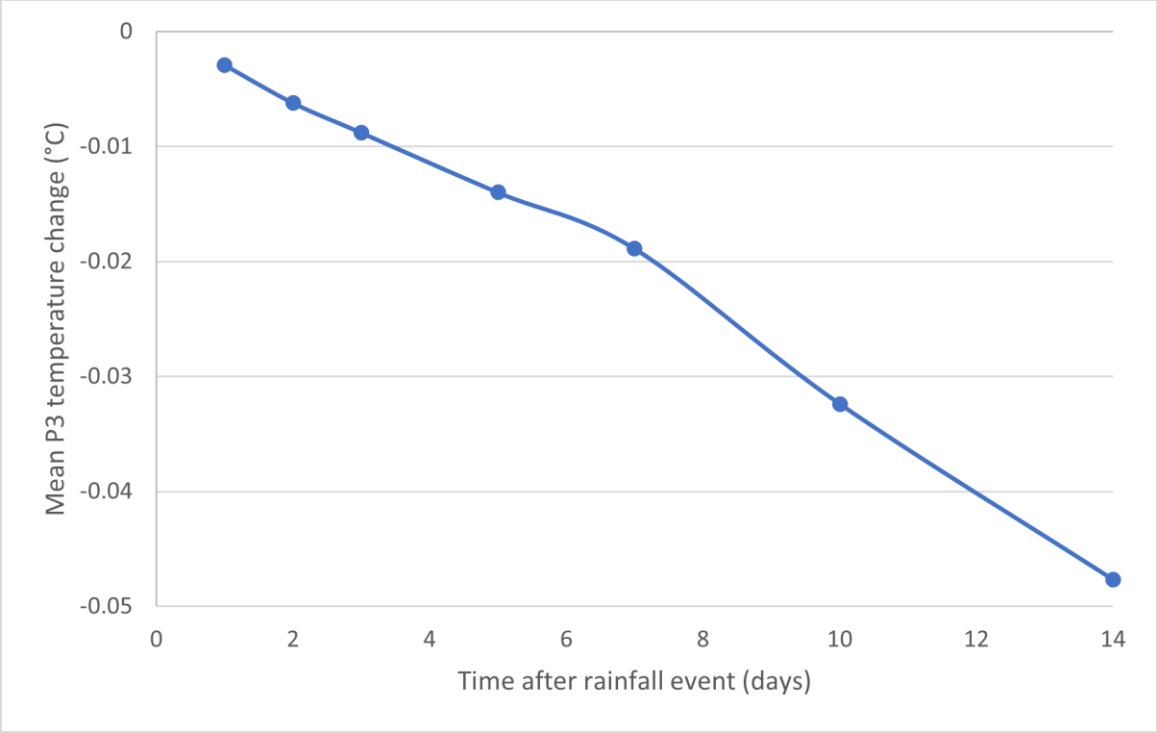


Figure 31. Mean change in P3 groundwater temperature following 25 rainfall events with total precipitation ≥5 mm. Temperature changes are expressed relative to the mean P3 temperature during the six hours preceding each event. Elaborated by the author.

4.1.4 Spatial distribution of mean groundwater temperature

The spatial distribution of mean groundwater temperature is shown in Figure 30. Clear differences were observed among the five monitoring points. P3 recorded the highest mean groundwater temperature (17.34 °C), followed by P1 (16.15 °C), whereas P5 recorded the lowest mean temperature (13.95 °C). P2 and P4 showed intermediate mean temperatures of 14.23 °C and 14.49 °C, respectively. These results indicate that groundwater temperature varies considerably among the individual monitoring locations. Since the five piezometers represent a limited monitoring network and show distinct site-specific behaviors, the observed spatial differences are not interpreted here as evidence of a general relationship between groundwater temperature and the degree of urbanization. Possible factors contributing to the behavior of individual monitoring points are considered separately in the Discussion.

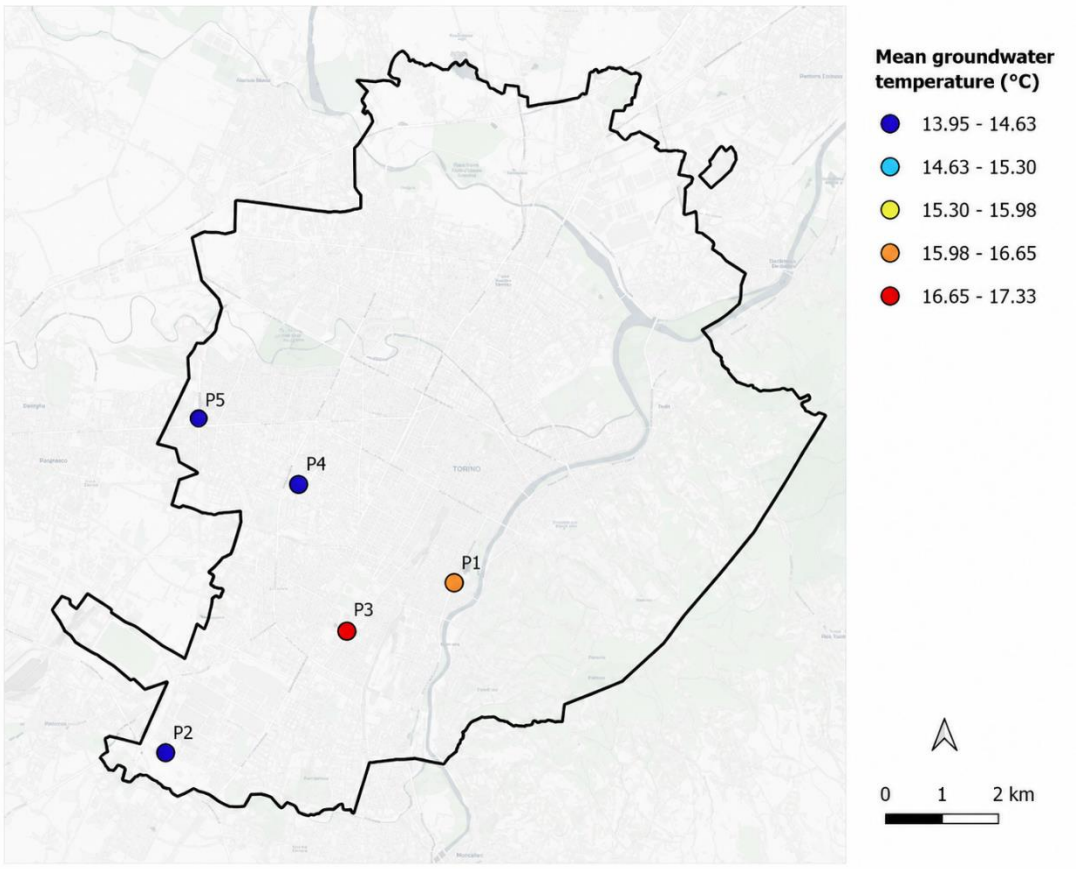


Figure 32. Spatial distribution of mean groundwater temperature at the five monitored piezometers in Turin.

4.2 Groundwater temperature characteristics across different urban contexts

4.2.1 Classification of the monitoring points by urban context

The five monitoring points were characterized according to the dominant land use and built-environment characteristics within a 200 m buffer around each piezometer. Based on these spatial characteristics, P1, P3, P4, and P5 were identified as predominantly urban locations, while P2 represented a less urban context. This classification is used to describe the local setting of each monitoring point rather than to establish a direct relationship between urban characteristics and groundwater temperature (Table 7).

Piezometer	Mean temperature (°C)	Dominant land use	Building context	Urban category
P1	16.15	Dense residential with industrial/commercial areas and major road infrastructure	Predominantly built-up urban fabric	**Urban**
P2	14.23	Mixed land use, with dense residential areas, road infrastructure, and a large share of non-irrigated agricultural/open land	Mixed built-up and open areas, with lower urban continuity	**Less urban**
P3	17.33	Dense residential with major road infrastructure and industrial/commercial areas	Dense and continuous built-up urban fabric	**Urban**
P4	14.49	Predominantly dense residential, with some low-density residential and road infrastructure	Predominantly built-up residential fabric	**Urban**
P5	13.95	Industrial/commercial land use, associated with dense and low-density residential areas and some urban green space	Mixed urban fabric with strong industrial/commercial presence	**Urban**

Table 8.Final urban-context classification of the five monitoring points, developed by the author based on GIS analysis of land-use and building-context characteristics.

The classification shows that P1, P3, P4, and P5 are located in predominantly urban contexts, although their surrounding land-use and building characteristics differ. P1 and P3 are characterized by dense built-up areas combined with major road infrastructure and industrial or commercial uses. P4 is mainly surrounded by dense residential development, while P5 presents a more heterogeneous urban context, including industrial and commercial areas, residential development, and some nearby green spaces. In contrast, P2 is classified as less urban because of the greater presence of open and non-irrigated agricultural land and lower continuity of the built-up fabric. Groundwater temperatures differed among the five monitoring points, including among locations classified within the same urban category. The urban-context classification is therefore used only to describe the spatial characteristics of the monitoring locations, while the temperature behavior of each piezometer is interpreted individually.

4.2.2 Building-height characteristics around the monitoring points

The building-height characteristics around the five monitoring points were examined within a 200 m buffer around each piezometer. The analysis identifies the dominant building-height classes and describes the surrounding built environment, providing additional spatial context for characterizing the local urban morphology of each monitoring point (Table 8).

Piezometer	Dominant building-height class	Building context
P1	2–7 floors, with some 8–18 floor buildings	Dense and continuous built-up fabric, characterized mainly by medium-rise buildings and the presence of some taller blocks
P2	Sparse built environment, with a limited number of 2–7 floor buildings and some 8–18 floor buildings	Low building density and discontinuous built-up fabric, with large open spaces around the monitoring point
P3	Mixed 4–7 and 8–18 floor buildings	Dense urban context with a combination of medium-rise and taller buildings along major roads
P4	4–7 floors	Predominantly dense residential fabric, mainly composed of medium-rise buildings with a few taller structures
P5	4–7 floors, with some 8–18 floor buildings	Mixed built environment with medium-rise buildings, some taller structures, and a less continuous urban fabric compared with the more compact sites

Table 9.Building-height characteristics within the 200 m buffer area around the five monitoring points, interpreted by the author based on GIS analysis of building-height classes.

The comparison shows clear differences in the built environment surrounding the monitoring points. P1, P3, and P4 are located within relatively dense urban fabrics, with P3 showing a greater presence of taller buildings. P5 also includes medium-rise and taller buildings, although its surrounding built environment is less continuous and more heterogeneous. In contrast, P2 is characterized by lower building density, a more discontinuous built-up fabric, and larger open spaces within the 200 m buffer. These differences provide a descriptive comparison of the built environment surrounding the five monitoring points and highlight the variation in urban morphology among the selected locations.

4.2.3 Urban-context classification of the monitoring points

The final urban-context classification was developed primarily from the dominant land-use characteristics, the continuity of the built-up fabric, and the presence of open or agricultural areas within the 200 m buffer around each piezometer. Monitoring points characterized by continuous built-up areas and predominantly residential, commercial, or infrastructure-related land uses were classified as urban. In contrast, locations with lower building coverage, larger open or agricultural areas, and a more discontinuous built environment were classified as less urban (Table 9).

Piezometer	Mean temperature (°C)	Land-use characteristics	Built-environment characteristics	Final urban category
P1	16.15	Dense residential and industrial/commercial land uses, with extensive road infrastructure	Dense and continuous built-up fabric	Urban
P2	14.23	Mixed land use with dense residential areas, infrastructure, and a substantial share of open or agricultural land	Low and discontinuous building coverage, with large open areas	Less urban
P3	17.33	Dense residential, industrial/commercial land uses, and major road infrastructure	Dense and continuous urban fabric with major road infrastructure	Urban
P4	14.49	Predominantly dense residential land use with limited green space	Continuous and predominantly residential built-up fabric	Urban
P5	13.95	Strong industrial/commercial presence, mixed residential land use, and some urban green areas	Mixed built environment with a less continuous urban fabric	Urban

Table 10. Final urban-context classification of the five monitoring points, developed by the author based on GIS analysis of land-use and built-environment characteristics within the 200 m buffer areas.

The combined classification indicates that P1, P3, P4, and P5 are located in urban contexts, although their surrounding built environments differ in density, continuity, and land-use composition. P1 and P3 are characterized by dense built-up areas and major infrastructure. P4 is also urban but is mainly characterized by continuous residential development, while P5 presents a more heterogeneous urban fabric with industrial and commercial uses and a less continuous built environment. In contrast, P2 is classified as less urban because of its lower building density and greater presence of open or agricultural land.

4.2.4 Groundwater temperature comparison between urban and less urban contexts

To descriptively compare groundwater temperature across the different monitoring contexts, the monitoring points were grouped according to the classification presented above. P1, P3, P4, and P5 were classified as urban, while P2 represented the less urban context (Table 10 and Figure 31).

Urban context	Monitoring points	Mean groundwater temperature (°C)
Urban	P1, P3, P4, P5	15.48
Less urban	P2	14.23

Table11.Comparison of mean groundwater temperature between urban and less urban monitoring contexts, calculated by the author based on the final urban-context classification

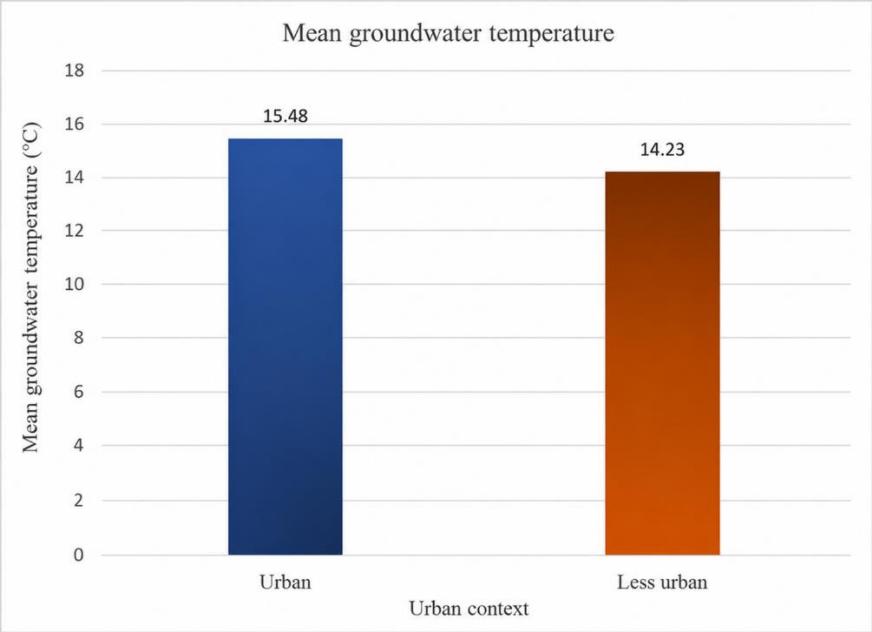


Figure 33.Comparison of mean groundwater temperature between urban and less urban monitoring contexts, calculated by the author

Within the monitored dataset, the mean groundwater temperature calculated for P1, P3, P4, and P5 was 15.48 °C, while P2 recorded a mean temperature of 14.23 °C, corresponding to a difference of approximately 1.25 °C. However, this comparison should be interpreted with caution because the less urban category is represented by only one monitoring point (P2), while considerable temperature differences are also observed among the individual urban sites. The observed difference therefore represents a site-specific pattern within the present monitoring network and should not be generalized as evidence of a direct relationship between urbanization and groundwater temperature.

4.2.5 Temporal comparison among the monitored contexts

To descriptively compare groundwater-temperature variations during the common monitoring period from December 2024 to May 2025, the monthly mean temperature of P1, P3, P4, and P5 was calculated and compared with the corresponding monthly temperature recorded at P2. This comparison was limited to the common monitoring period to ensure temporal consistency among the five monitoring points. The monthly temperature difference (ΔT) was calculated as the difference between the mean of P1, P3, P4, and P5 and the corresponding temperature at P2, following standard descriptive-statistical procedures (Walpole et al., 2012).

$$\{T\}_{\{Group,m\}} = \frac{T_{\{P1,m\}} + T_{\{P3,m\}} + T_{\{P4,m\}} + T_{\{P5,m\}}}{4}$$

$$\Delta T_m = \{T\}_{\{urban,m\}} - T_{\{P2,m\}}$$

T̄ group, m= mean groundwater temperature of the urban monitoring points in month m (°C);
TP1,m = groundwater temperature at P1 in month m (°C);
TP3,m = groundwater temperature at P3 in month m (°C);
TP4,m = groundwater temperature at P4 in month m (°C);
TP5,m = groundwater temperature at P5 in month m (°C);
TP2,m = groundwater temperature at the less urban monitoring point P2 in month m (°C);
ΔTm = difference between T̄ group, m and the groundwater temperature recorded at P2 in month m (°C).
Positive values of ΔTm indicate that the mean groundwater temperature calculated for P1, P3, P4, and P5 was higher than the temperature recorded at P2 during the same month. (Table 11).

Month	Urban mean (°C)	Less urban, P2 (°C)	Difference (°C)
24-Dec	15.55	14.23	1.32
25-Jan	15.59	14.22	1.36
25-Feb	15.56	14.22	1.34
25-Mar	15.55	14.22	1.32
25-Apr	15.50	14.23	1.28
25-May	15.44	14.24	1.20

Table 12. Monthly comparison of groundwater temperature between urban and less urban monitoring contexts during the common monitoring period, calculated by the author from the groundwater temperature dataset.

Figure 34 illustrates the temporal evolution of the monthly mean groundwater temperatures in the two monitoring contexts, allowing the persistence and variation of the thermal difference to be visually compared over time.

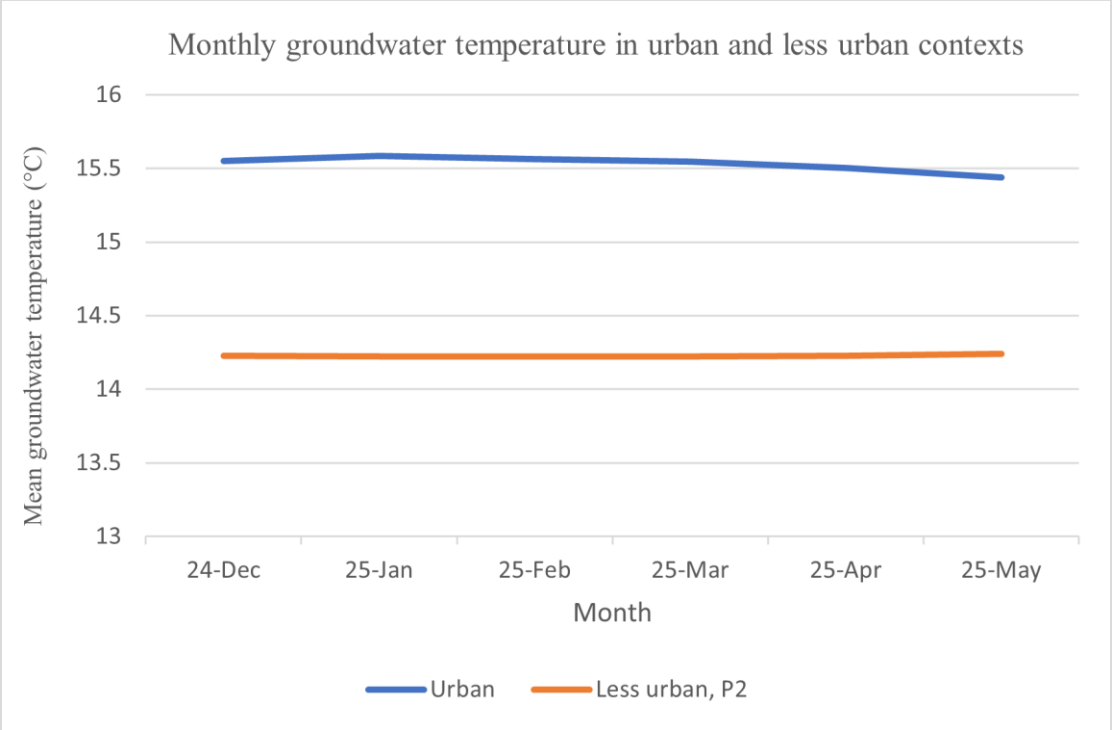


Figure 34. Monthly groundwater temperature comparison between urban and less urban monitoring contexts during the common monitoring period, calculated by the author from the groundwater temperature dataset.

During the common monitoring period, the monthly mean calculated for P1, P3, P4, and P5 remained higher than the corresponding temperature recorded at P2. The difference ranged from approximately 1.20 °C in May 2025 to 1.36 °C in January 2025. This comparison represents a descriptive pattern within the monitored dataset and should not be interpreted as a general urban–less urban thermal relationship.

4.3 Spatial and Environmental Data Sources:

Most of the spatial datasets for this study came from the Geoportale Piemonte regional geoportal. Additional open-access sources, such as OpenStreetMap and the Copernicus Urban Atlas, were also used.

Table 12 summarizes the spatial and environmental datasets used in this study, including their original sources, data types, and the main processing steps applied before the analysis. The datasets include groundwater monitoring data as well as spatial information on land use, buildings, topography, transport infrastructure, urban green areas, and climate. In addition, the table identifies the datasets derived specifically for this study, including the 200 m buffer areas and the final urban-context classification.

Dataset	Original source	Original data type	Status in this study	Processing or editing performed
Turin municipal boundary	Geoportale Piemonte	Polygon vector	Processed/edited	Reprojected to the common coordinate system and used to delimit the study area
Piezometer locations	Groundwater monitoring dataset	Point vector / coordinates	Processed/edited	Imported into QGIS, georeferenced, labelled as P1–P5
Groundwater temperature data	Monitoring sensors	Time-series data	Processed/edited	Cleaned, organized by monitoring point, and aggregated to calculate descriptive statistics and monthly mean temperatures
Building footprints	Geoportale Piemonte / OpenStreetMap	Polygon vector	Processed/edited	Clipped to the 200 m buffer areas and used to characterize the surrounding built-up fabric
Building height and number of floors	CLoP dataset / OpenStreetMap attributes	Polygon attributes	Processed/edited	Classified into building-height categories and clipped to the 200 m buffer surrounding each piezometer
Land-use data	Copernicus Urban Atlas / regional land-use dataset	Polygon vector	Processed/edited	Reclassified into common land-use categories and clipped to the 200 m buffer around each monitoring point
Digital Elevation Model	Geoportale Piemonte	Raster	Processed	Reprojected and used for the topographic characterization of the study area
Satellite imagery	Google Satellite	Raster basemap	Original/reference layer	Used as a visual reference and cartographic basemap; no thematic reclassification was performed
Road and transport network	OpenStreetMap	Line and polygon vector	Processed/edited	Extracted and incorporated into the land-use and infrastructure classification
Urban green areas	Copernicus Urban Atlas / OpenStreetMap	Polygon vector	Processed/edited	Extracted, reclassified, and included in the land-use maps
Climate data	ARPA Piemonte	Time-series data	Processed	Selected and summarized to describe the climatic characteristics of Turin
200 m buffer areas	Derived in this study	Polygon vector	Derived dataset	Generated around each piezometer to define a consistent spatial analysis area
Urban-context classification	Derived from land use and building height	Thematic classification	Derived dataset	Developed by combining land-use composition, building density, and building-height characteristics

Table 13. Spatial and environmental datasets used and processed in this study, including original data sources, data types, and GIS processing steps.

4.4 GIS Environment and Spatial Processing:

Spatial data processing, analysis, and map production were carried out using QGIS, an open-source Geographic Information System (GIS) that supports the management, visualization, analysis, and integration of both vector and raster spatial datasets. QGIS was selected as the main GIS environment because it allowed datasets obtained from different sources and formats to be processed within a common spatial framework and combined for the characterization of the groundwater monitoring locations.

As a first step, the spatial datasets were imported into QGIS and checked for their coordinate reference systems. To ensure spatial consistency among all layers, the datasets used for the analysis were transformed, where necessary, to WGS 84 / UTM Zone 32N (EPSG:32632). The locations of the five piezometers (P1–P5) were then georeferenced and used as the reference points for the subsequent spatial analyses.

A 200 m buffer was generated around each piezometer to define a consistent spatial analysis area for characterizing the surrounding urban environment. Building footprints, building-height information, land-use classes, road infrastructure, and urban green areas were clipped to these buffer zones. The original land-use categories obtained from different spatial datasets were subsequently reclassified into a common classification scheme to facilitate comparison among the monitoring points.
Building information was processed to characterize both the density and height of the built environment surrounding each piezometer. Building-height attributes were grouped into representative height classes, while the spatial distribution and continuity of the built-up fabric were visually and quantitatively examined within each buffer. These results were combined with the land-use analysis to distinguish monitoring points characterized by dense and continuous urban development from locations with a greater presence of open or agricultural land.
Groundwater temperature information was linked to the corresponding piezometer locations and incorporated into the GIS environment to examine its spatial distribution across Turin. Groundwater temperatures were represented cartographically to examine their spatial distribution across the monitoring network. The surrounding land-use and built-environment characteristics were used separately to describe the local urban context of each monitoring point.

This workflow ensured that all monitoring points were evaluated using the same spatial extent, coordinate system, and classification criteria, providing a consistent basis for describing both groundwater-temperature patterns and the surrounding urban context.

Chapter 5 – Discussion

5.1 Interpretation of groundwater temperature variability in an urban context

Groundwater in cities is often discussed mainly in relation to contamination and water quality, while its thermal alteration receives less attention. However, urban development can modify subsurface temperature through several processes, including heat exchange with buildings and basements, heating and cooling systems, underground infrastructure, paved surfaces, traffic-related heat, and other anthropogenic sources. For this reason, groundwater temperature can be considered an additional indicator of how the urban environment interacts with the shallow subsurface.

The monitoring results show that groundwater temperature did not respond uniformly across the five piezometers. P2, P4, and P5 remained comparatively stable throughout their monitoring periods, whereas P3 displayed substantially greater temporal variability and a distinct seasonal pattern. P1 also showed limited variability, although this observation should be interpreted cautiously because its monitoring record covered only part of the annual cycle, from December 2024 to May 2025. The absence of a complete summer and autumn period makes it difficult to determine whether a stronger seasonal signal would have developed at P1 over a full year.

A relevant reference for interpreting these results is the study conducted in Milan by Previati and Crosta (2021). Their analysis identified groundwater-temperature anomalies of up to approximately 3 °C and demonstrated considerable spatial variability in subsurface thermal conditions within the urban environment. Although the monitoring design, spatial coverage, and hydrogeological setting of Milan differ from those of the present study, their findings provide a useful regional example showing that groundwater temperature within urban areas can be spatially heterogeneous. The comparison should therefore be considered contextual rather than quantitative, particularly given the limited number of monitoring points available in Turin.

P3 showed the clearest temporal variability among the five monitoring points. Groundwater temperature decreased progressively during spring and summer, reaching a minimum monthly mean of approximately 16.61 °C in August 2025, before increasing again during autumn and winter to approximately 17.82 °C in January 2026. This seasonal behavior is particularly noteworthy because the minimum groundwater temperature occurred during summer and the maximum during winter, indicating a temporal pattern that differs from the typical seasonal cycle of surface air temperature.

To investigate whether precipitation could contribute to the distinct temporal behavior observed at P3, the groundwater-temperature record was examined together with precipitation data. No significant contemporaneous relationship was identified between daily precipitation and absolute P3 groundwater temperature, and correlations with subsequent absolute temperature remained negligible across lags of

0–30 days. However, a different pattern emerged when daily temperature changes were considered. A weak negative association was observed approximately 7–11 days after precipitation, with the strongest Pearson correlation at a lag of 10 days ($r = -0.201$) and the strongest Spearman correlation at a lag of 8 days ($\rho = -0.270$). Although statistically detectable after correction for multiple testing, the magnitude of these associations was small, with the 10-day Pearson relationship accounting for approximately 4% of the variance in daily temperature change.

The rainfall-event analysis provided complementary evidence of a delayed but weak temperature response. Across the 25 rainfall events analyzed, mean P3 temperature change was almost negligible one day after rainfall and became progressively more negative over the following days, reaching approximately −0.032 °C after 10 days and −0.048 °C after 14 days. However, these event-based differences did not remain statistically significant after correction for multiple testing. Taken together, the correlation and event-based analyses indicate that precipitation is associated with only a weak and delayed component of short-term P3 temperature variability, rather than with a dominant or immediate response.

One possible interpretation of the observed lag is a delayed recharge-related response. Precipitation infiltrating through the unsaturated zone may influence groundwater temperature after a delay, while heat exchange within the soil and unsaturated zone, groundwater mixing, and local flow conditions may further modify the thermal signal before it is detected at the monitoring point. The approximately 8–10-day lag identified in this study should therefore not be interpreted directly as groundwater travel time. Nevertheless, the delayed negative association is consistent with the possibility that recharge processes contribute to short-term cooling at P3. Confirmation of this mechanism would require additional information on groundwater levels, recharge rates, unsaturated-zone properties, and local groundwater-flow conditions.

Other site-specific influences cannot be excluded. In particular, local subsurface infrastructure or geothermal heating and cooling systems could potentially modify groundwater temperature independently of meteorological forcing. Such anthropogenic thermal inputs could contribute to the distinctive temporal behavior observed at P3, but their presence, location, and operating conditions were not available in the present dataset. Consequently, geothermal interference remains a possible explanation rather than a demonstrated mechanism. Distinguishing between recharge-related effects, groundwater-flow controls, and anthropogenic thermal influences would require additional hydrogeological information and site-specific data on subsurface infrastructure and geothermal installations.

The inverse seasonal pattern observed at P3 represents one of the most distinctive findings of this study. Although the precipitation analysis identified a weak delayed response, the available data are not sufficient to fully explain the mechanisms responsible for this behavior. A longer monitoring period and a more detailed investigation of the area surrounding P3 would therefore be valuable. In particular, future research should examine nearby subsurface infrastructure, geothermal installations, building energy systems, and other local activities that could potentially influence groundwater thermal conditions, together with more detailed hydrogeological information. This would help determine whether the unusual seasonal pattern at P3 is mainly related to recharge and groundwater dynamics, local anthropogenic thermal influences, or a combination of these processes.

In contrast, P2, P4, and P5 showed considerably weaker temporal variability than P3. P2, representing the less urban monitoring context, remained particularly stable, while P4 also showed limited variation despite its dense residential setting. P5 recorded the lowest mean groundwater temperature among the five monitoring points despite being classified as an urban site. These contrasting observations reinforce the importance of interpreting each monitoring point individually and indicate that the observed groundwater-temperature patterns cannot be explained solely by the urban-context classification used in this study.

A descriptive comparison between the four monitoring points classified as urban and P2 provides additional context for these site-specific differences. The mean groundwater temperature calculated for P1, P3, P4, and P5 was approximately 15.48 °C, compared with 14.23 °C at P2, corresponding to a difference of approximately 1.25 °C. However, this difference should not be interpreted as evidence of a general urban–less urban thermal relationship, because the less urban category is represented by only one monitoring point and substantial variability is also present among the four urban sites. The comparison therefore represents a local pattern within the present monitoring network rather than a general effect of urbanization on groundwater temperature.

The main contribution of this study lies in the integration of continuous groundwater-temperature monitoring with a site-specific GIS-based characterization of the surrounding urban environment. Land use, building height, built-up continuity, and open-space characteristics were examined within a consistent 200 m buffer around each piezometer to provide a standardized description of the local urban context. Rather than establishing direct relationships between individual urban variables and groundwater temperature, this framework allows the thermal behavior of each monitoring point to be considered within its specific spatial setting. The results particularly demonstrate the importance of considering individual monitoring locations, as substantial differences were observed even among sites assigned to the same urban-context category. Ferguson and Woodbury (2007) showed that subsurface temperature patterns can vary considerably within urban areas and are not necessarily controlled by surface land use alone. This is consistent with the results observed at P5, which recorded the lowest mean groundwater temperature despite being classified as an urban monitoring point. The thermal

influence of urbanization may also reflect the historical development of the built environment. In Amsterdam, Visser et al. (2020) reported higher subsurface temperatures in urban areas than in surrounding rural areas and related the development of the subsurface urban heat island to long-term urban growth.

These studies provide broader evidence that groundwater-temperature patterns in urban environments may reflect the combined influence of long-term urban development, subsurface conditions, and local site characteristics. Such factors may also be relevant when considering the differences observed among the Turin monitoring points, although their individual contributions could not be quantified in the present study.

This interpretation is also relevant to the Piedmont Po Plain, where long-term observations have shown that groundwater temperature can vary over time under the combined influence of climatic and local environmental conditions (Lasagna et al., 2024). This regional evidence provides an important context for the Turin monitoring results, indicating that the observed groundwater temperature patterns should be interpreted within the broader hydrogeological and climatic setting of the Po Plain.

Because the monitoring period of this study was relatively short, long-term climate-related trends could not be evaluated. The findings therefore primarily characterize spatial differences and short-term temporal variability within the monitoring network rather than long-term groundwater warming.

5.2 Implications for urban planning and groundwater management

The groundwater-temperature variability observed among the five monitoring locations has relevant implications for urban planning and groundwater management. The results indicate that shallow subsurface thermal conditions can vary substantially within the same urban area. Groundwater temperature should therefore be considered as a local environmental parameter rather than as a uniform characteristic of the urban aquifer.

From an urban-planning perspective, subsurface thermal information may complement conventional spatial and environmental assessments, particularly for projects involving underground structures, transport infrastructure, utility networks, and shallow geothermal systems. The present results do not establish direct relationships between specific urban characteristics and groundwater temperature, but they highlight the importance of considering subsurface thermal conditions as an additional component of urban environmental assessment.

The observed spatial differences also underline the importance of maintaining a distributed groundwater-monitoring network. Measurements from a single monitoring point cannot adequately

represent the thermal variability of the urban aquifer. Regular monitoring of groundwater temperature, water levels, and relevant hydrochemical parameters can help distinguish seasonal variability from longer-term thermal trends and can support the identification of possible anthropogenic thermal impacts.

Groundwater-temperature data are also relevant for the planning and management of shallow geothermal plants. Urban aquifers can provide a low-temperature energy resource for heating and cooling, but the operation of several geothermal plants within the same area may lead to thermal interference if their location, extraction rates, and reinjection conditions are not properly coordinated. One possible strategy is to integrate geothermal energy and recovered waste heat into existing or newly developed district heating and cooling networks. In such systems, thermal energy can be collected from centralized or distributed heat and cold sources and transferred to users through a network of pipelines, allowing a more coordinated use of subsurface thermal resources and reducing the risk of local thermal imbalance.

Elevated groundwater temperatures can, in some urban settings, be associated with subsurface thermal anomalies and may represent a potential low-temperature energy resource. However, groundwater temperature alone is insufficient to identify a subsurface urban heat-island effect or to determine the feasibility of thermal-energy exploitation. Such assessments require additional information on hydrogeological conditions, groundwater flow, aquifer properties, thermophysical characteristics, groundwater chemistry, background thermal conditions, and existing underground infrastructure. These factors are necessary both to characterize subsurface thermal anomalies and to evaluate the suitability of the aquifer for geothermal applications.

The present results further indicate that groundwater-temperature patterns should be interpreted together with site-specific environmental and hydrogeological information rather than on the basis of urban characteristics alone. The GIS-based land-use and built-environment analysis provides useful spatial context for describing the monitoring locations, but direct relationships between these characteristics and groundwater temperature were not established in this study. A more comprehensive assessment would require groundwater-temperature records to be combined with information on groundwater levels, aquifer properties, flow conditions, geology, underground infrastructure, and existing geothermal installations. The P3 analysis further illustrates the importance of considering meteorological and hydrogeological processes when interpreting groundwater-temperature variability. The weak delayed association observed between precipitation and subsequent temperature change suggests that short-term groundwater thermal responses may occur several days after meteorological forcing rather than immediately. Although the detected relationship was small and cannot establish a specific recharge mechanism, it indicates that precipitation and recharge-related processes should be considered alongside urban and anthropogenic factors when evaluating groundwater-temperature

records. Future monitoring strategies would therefore benefit from integrating groundwater temperature with precipitation, groundwater-level, and, where possible, recharge and flow observations.

Based on the findings and limitations of this study, the following actions are suggested to support future groundwater monitoring and subsurface planning in Turin:

1. Maintain and progressively expand the groundwater-temperature monitoring network to include a wider range of urban, peri-urban, and less urban settings, as well as different hydrogeological conditions.
2. Combine groundwater-temperature monitoring with precipitation, groundwater-level, and, where possible, groundwater-flow observations to better distinguish meteorological, hydrogeological, and anthropogenic controls on temporal variability.

3. Integrate groundwater-temperature and hydrogeological information into municipal GIS and subsurface-planning tools.

4. Assess the cumulative thermal effects of major construction projects, underground infrastructure, and shallow geothermal plants before implementation.

5. Establish baseline groundwater-temperature conditions before approving new shallow geothermal installations.
6. Promote coordination among groundwater management, urban planning, and energy planning, including the possible integration of geothermal energy and recovered excess heat into district heating and cooling networks, in order to reduce thermal interference and support a more efficient use of subsurface thermal resources.

These actions would support both environmental protection and urban-energy planning by providing a more coordinated framework for managing subsurface thermal conditions.

Figure 35 presents a conceptual framework illustrating potential interactions among urban development, anthropogenic heat sources, shallow groundwater thermal conditions, and geothermal management. The framework is intended to provide a general interpretation of the processes discussed in the literature and does not represent causal relationships demonstrated by the present monitoring dataset.

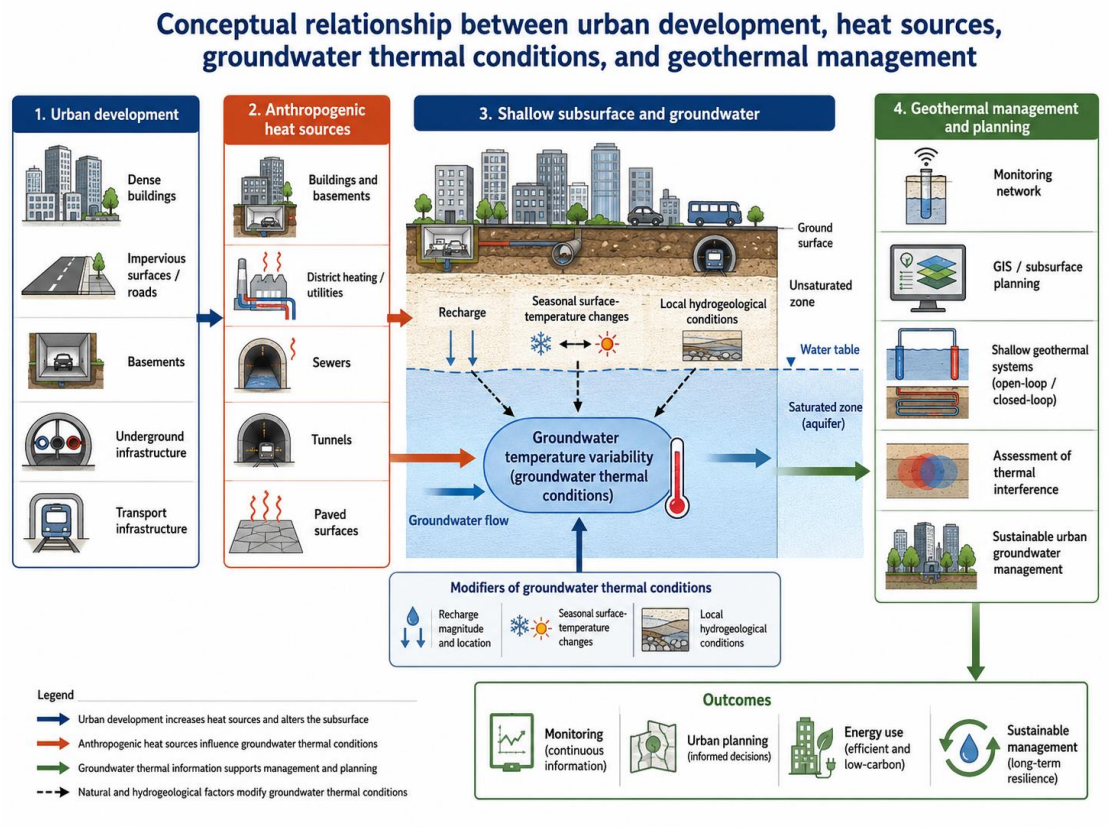


Figure 35. Conceptual framework of potential interactions among urban development, anthropogenic heat sources, groundwater thermal conditions, and geothermal management. Elaborated by the author.

5.3 Limitations and future research activities

This study provides an initial assessment of groundwater-temperature variability across five monitoring points in Turin; however, several limitations should be considered when interpreting the results. The monitoring network is relatively small and does not provide uniform spatial coverage of the entire municipal area. In particular, P1, P3, P4, and P5 were classified as urban monitoring points, while P2 was the only site representing a less urban context. Consequently, the comparison between urban and fewer urban conditions is based on an unbalanced number of monitoring locations and should not be generalized to the whole city.

Differences in monitoring duration also affect direct comparisons among the piezometers. P1 had the shortest monitoring record because of sensor-related limitations, whereas the other monitoring points covered longer periods. In addition, although measurements affected by sensor removal, reinsertion, and stabilization were excluded from the analysis, information on the exact installation depth of the Mini-Diver sensors was not available. It was therefore not possible to independently verify whether the sensor depth remained completely consistent throughout the monitoring period. This limitation is particularly relevant when interpreting temporal variability and comparing the response of different monitoring points.

The available dataset also did not include sufficiently detailed hydrogeological information to quantify the influence of individual controls on groundwater temperature. Parameters such as groundwater level, flow direction and velocity, aquifer thickness, hydraulic properties, recharge conditions, and the location of underground infrastructure can influence heat transport within the subsurface. The detailed analysis of P3 identified a weak negative association between precipitation and subsequent daily temperature change, with the clearest signal occurring approximately 8–10 days after rainfall. However, this lag cannot be interpreted directly as groundwater travel time or as evidence of a specific recharge mechanism because groundwater-level, recharge-rate, unsaturated-zone, and local groundwater-flow data were not available. Similarly, information on the location and operation of geothermal systems and other potential anthropogenic heat sources was insufficient to determine whether they contributed to the distinctive behavior observed at P3. The individual contributions of these processes therefore could not be quantified using the available dataset.

Future research should first extend the groundwater-temperature monitoring network to include a larger number of sites representing a wider range of urban, peri-urban, and less urban conditions. Longer and more homogeneous monitoring periods would allow seasonal and interannual variability to be evaluated more reliably and would make it possible to distinguish persistent thermal anomalies from short-term fluctuations. Temperature measurements should also be combined with systematic observations of precipitation, groundwater level, groundwater flow, recharge conditions, and hydrochemical parameters. At P3 in particular, simultaneous high-frequency monitoring of groundwater temperature and groundwater level would help determine whether the approximately 8–10-day delayed temperature response identified after precipitation is associated with recharge and groundwater dynamics. Information on nearby geothermal installations, underground infrastructure, and other potential anthropogenic thermal sources would also be necessary to evaluate alternative explanations for the distinctive P3 pattern.

A further development would be the construction of an integrated spatial database combining groundwater-temperature measurements with hydrogeological, geological, land-use, building,

infrastructure, and energy-related information. Such an approach would support more detailed identification of areas potentially affected by subsurface urban heat islands and would help distinguish the contribution of different natural and anthropogenic heat sources. Three-dimensional groundwater-flow and heat-transport modelling could then be used to reproduce the spatial and temporal evolution of groundwater temperatures and to test different urban-development and climate scenarios.

Future analyses should also evaluate the thermophysical and chemical characteristics of the aquifer in greater detail. These data would improve the assessment of both the intensity of possible subsurface urban heat islands and the suitability of groundwater for shallow geothermal applications. In particular, detailed modelling could help estimate the available thermal resource, identify areas at risk of thermal interference, and support the spatial planning of new geothermal plants.

At the urban scale, future research should increasingly connect groundwater management with energy and spatial planning. This could include evaluating the integration of shallow geothermal resources and recovered excess heat into district heating and cooling networks, improving the thermal energy efficiency of public and private buildings, and assessing the cumulative subsurface thermal effects associated with industrial, agricultural, transport, and infrastructure activities. A more integrated representation of the urban subsoil and groundwater system would therefore provide a stronger basis for sustainable resource management, thermal-energy planning, and regulation of subsurface uses.

Overall, the present study should be considered a site-specific assessment of groundwater thermal conditions within a limited monitoring network in Turin. Expanding the monitoring network, extending the temporal coverage, improving hydrogeological characterization, and integrating meteorological, groundwater-level, and subsurface-infrastructure information would allow future studies to determine more clearly the relative importance of recharge processes, groundwater dynamics, urban development, subsurface infrastructure, and climatic forcing in controlling groundwater-temperature patterns across the city. Integrated groundwater-flow and heat-transport modelling could subsequently be used to test these processes more explicitly.

Chapter 6 – Conclusions

The results of this study show clear spatial and temporal variability in groundwater temperature among the five monitoring points in Turin. Mean groundwater temperatures ranged from 13.95 °C at P5 to 17.34 °C at P3, corresponding to a difference of approximately 3.39 °C within the monitoring network. P3 recorded the highest mean temperature and the strongest temporal variability, whereas P2, P4, and P5 remained comparatively stable during their monitoring periods. P1 also showed limited variability, although its shorter monitoring record should be considered when making direct comparisons.

P3 was particularly distinct, showing a seasonal pattern characterized by lower groundwater temperatures in summer and higher values in winter, with the minimum monthly mean occurring in August and the maximum in January. The precipitation analysis identified no significant immediate relationship between rainfall and absolute P3 groundwater temperature. However, a weak negative association was observed between precipitation and subsequent daily temperature changes, with the clearest lagged signal occurring approximately 8–10 days after rainfall. The strongest Pearson correlation occurred at a lag of 10 days ($r = -0.201$), while the strongest Spearman correlation occurred at a lag of 8 days ($\rho = -0.270$). These associations were statistically detectable but small in magnitude, and the rainfall-event analysis did not remain statistically significant after correction for multiple testing. The results therefore indicate a weak delayed association with precipitation rather than a dominant or immediate meteorological control on P3 temperature variability.

The distinct inverse seasonal pattern observed at P3 is particularly noteworthy and warrants further investigation through longer-term monitoring and a more detailed assessment of hydrogeological conditions and potential thermal activities in the surrounding area.

The GIS-based analysis classified P1, P3, P4, and P5 as urban monitoring points, while P2 represented a less urban context. The mean groundwater temperature calculated for P1, P3, P4, and P5 was approximately 15.48 °C, compared with 14.23 °C at P2, corresponding to a difference of about 1.25 °C. However, this comparison represents only a local pattern within the present monitoring network because the less urban category is represented by a single monitoring point and substantial temperature differences also occur among the urban sites. The observed contrast therefore should not be interpreted as evidence of a general urban–less urban thermal relationship or of a city-wide subsurface urban heat-island effect.

Groundwater-temperature behavior differed substantially among individual monitoring points, including sites assigned to the same urban-context category. P5 recorded the lowest mean groundwater temperature despite its urban classification, whereas P3, also located in an urban setting, recorded the highest mean temperature and the strongest temporal variability. These observations indicate that the

urban-context classification used in this study is not sufficient to explain the observed thermal patterns. Instead, the observed thermal behavior is likely influenced by a combination of site-specific factors, including groundwater flow, aquifer properties, recharge processes, monitoring conditions, underground infrastructure, and other local thermal influences. The delayed precipitation–temperature association at P3 may reflect a recharge-related contribution to short-term variability; however, the available data are insufficient to distinguish this process from other hydrogeological or anthropogenic influences.

Taken together, the findings highlight the value of combining continuous groundwater-temperature monitoring with GIS-based characterization of the surrounding urban environment. The site-specific analysis of land use, building height, built-up continuity, and open-space characteristics within a consistent 200 m buffer provides a standardized spatial description of each monitoring location. Rather than establishing direct relationships between individual urban characteristics and groundwater temperature, this approach supports a more contextual interpretation of the thermal behavior observed at each piezometer.

The results also emphasize the importance of extending the monitoring network and integrating groundwater-temperature records with precipitation, groundwater-level, hydrogeological, and subsurface-infrastructure information. Such integration would help distinguish recharge-related responses from other natural and anthropogenic influences and would provide a stronger basis for identifying thermal anomalies, evaluating shallow geothermal potential, and supporting future urban and groundwater-management strategies in Turin.

Chapter 7 – References

1. Anderson MP (2005) Heat as a ground water tracer. Ground Water 43:951–968.

2. Bayer P, Attard G, Blum P, Menberg K (2019) The geothermal potential of cities. Renewable and Sustainable Energy Reviews 106:17–30.

3. Beltrami H (2002) Climate from borehole data: Energy fluxes and temperatures since 1500. Geophysical Research Letters 29:2111.

4. Bense VF, Beltrami H (2007) Impact of horizontal groundwater flow and localized deforestation on the development of shallow temperature anomalies. Journal of Geophysical Research: Earth Surface 112: F04015.

5. Benz SA, Bayer P, Goettsche FM, Olesen FS, Blum P (2016) Linking surface urban heat islands with groundwater temperatures. Environmental Science & Technology 50:70–78.

6. Bonte M, Röling WFM, Zaura E, van der Wielen PWJJ, Stuyfzand PJ, van Breukelen BM (2013) Impacts of shallow geothermal energy production on redox processes and microbial communities. Environmental Science & Technology 47:14476–14484.

7. Bredehoeft JD, Papadopulos IS (1965) Rates of vertical groundwater movement estimated from the Earth’ s thermal profile. Water Resources Research 1:325–328.

8. Brielmann H, Griebler C, Schmidt SI, Michel R, Lueders T (2009) Effects of thermal energy discharge on shallow groundwater ecosystems. FEMS Microbiology Ecology 68:273–286.

9. Burns ER, Zhu Y, Zhan H, Manga M, Williams CF, Ingebritsen SE, Dunham JB (2017) Thermal effect of climate change on groundwater-fed ecosystems. Water Resources Research **53**:3341–3351.

10. Clauser C, Huenges E (1995) Thermal conductivity of rocks and minerals. In: Ahrens TJ (ed) Rock Physics and Phase Relations: A Handbook of Physical Constants. American Geophysical Union, Washington DC, pp 105–126.

11. Côté J, Konrad JM (2005) A generalized thermal conductivity model for soils and construction materials. Canadian Geotechnical Journal 42:443–458.

12. Egidio E, Mancini S, De Luca DA, Lasagna M (2022) The impact of climate change on groundwater temperature of the Piedmont Po Plain (NW Italy). Water 14:2797.

13. Epting J, Huggenberger P (2013) Unraveling the heat island effect observed in urban groundwater bodies: Definition of a potential natural state. Journal of Hydrology 501:193–204.

14. Ferguson G, Woodbury AD (2007) Urban heat island in the subsurface. Geophysical Research Letters 34: L23713.

15. Figura S, Livingstone DM, Hoehn E, Kipfer R (2011) Regime shift in groundwater temperature triggered by the Arctic Oscillation. Geophysical Research Letters 38: L23401.

16. Forno MG, De Luca DA, Bonasera M, Bucci A, Gianotti F, Lasagna M, Lucchesi S, Pelizza S, Taddia G, Piana F (2018) Synthesis on the Turin subsoil stratigraphy and hydrogeology (NW Italy). Alpine and Mediterranean Quaternary 31:147–169.

17. Garzena D, Acquaotta F, Fratianni S (2019) Analysis of the long-time climate data series for Turin and assessment of the city' s urban heat island.

18. Hannah DM, Malcolm IA, Bradley C (2009) Seasonal hyporheic temperature dynamics over riffle bedforms. Hydrological Processes 23:2178–2194.

19. Huang S, Pollack HN, Shen PY (2000) Temperature trends over the past five centuries reconstructed from borehole temperatures. Nature 403:756–758.

20. Jyrkama MI, Sykes JF (2007) The impact of climate change on spatially varying groundwater recharge in the Grand River watershed, Ontario. Journal of Hydrology 338:237–250.

21. Kurylyk BL, MacQuarrie KTB, McKenzie JM (2014) Climate change impacts on groundwater and soil temperatures in cold and temperate regions: Implications, mathematical theory, and emerging simulation tools. Earth-Science Reviews 138:313–334.

22. Kurylyk BL, MacQuarrie KTB, Voss CI (2014) Climate change impacts on the temperature and magnitude of groundwater discharge from shallow, unconfined aquifers. Water Resources Research 50:3253–3274.

23. Lasagna M, Egidio E, De Luca DA (2024) Groundwater Temperature Stripes: A Simple Method to Communicate Groundwater Temperature Variations Due to Climate Change. *Water* 16:717.

24. Menberg K, Bayer P, Zosseder K, Rumohr S, Blum P (2013) Subsurface urban heat islands in German cities. Science of the Total Environment 442:123–133.

25. Menberg K, Blum P, Kurylyk BL, Bayer P (2014) Observed groundwater temperature response to recent climate change. Hydrology and Earth System Sciences 18:4453–4466.

26. Menberg K, Blum P, Schaffitel A, Bayer P (2013) Long-term evolution of anthropogenic heat fluxes into a subsurface urban heat island. Environmental Science & Technology 47:9747–9755.

27. Neidhardt H, Shao W (2023) Impact of climate change-induced warming on groundwater temperatures and quality. Applied Water Science 13:235.

28. Oke TR (1982) The energetic basis of the urban heat island. Quarterly Journal of the Royal Meteorological Society 108:1–24.

29. Pollack HN, Huang S, Shen PY (1998) Climate change record in subsurface temperatures: a global perspective. Science 282:279–281.

30. Previati A, Crosta GB (2021) Characterization of the subsurface urban heat island and its sources in the Milan city area, Italy. Hydrogeology Journal ***29****:2487–2500.*

31. Taniguchi M, Burnett WC, Cable JE, Turner JV (2002) Investigation of submarine groundwater discharge. Hydrological Processes 16:2115–2129.

32. Taniguchi M, Uemura T (2005) Effects of urbanization and groundwater flow on subsurface temperature in Osaka, Japan. Physics of the Earth and Planetary Interiors 152:305–313.

33. Taniguchi M, Uemura T, Jago-on K (2007) Combined effects of urbanization and global warming on subsurface temperature in four Asian cities. Vadose Zone Journal 6:591–596.

34. Taylor CA, Stefan HG (2009) Shallow groundwater temperature response to climate change and urbanization. Journal of Hydrology 375:601–612.

35. Visser PW, Kooi H, Bense V, Boerma E (2020) Impacts of progressive urban expansion on subsurface temperatures in the city of Amsterdam (The Netherlands). Hydrogeology Journal 28:1755–1772.

36. Zhu K, Bayer P, Grathwohl P, Blum P (2015) Groundwater temperature evolution in the subsurface urban heat island of Cologne, Germany. Hydrological Processes 29:965–978.